CELL BIOLOGY

Citrulline regulates macrophage metabolism and inflammation to counter aging in mice

Zhangdan Xie[1,2]†, Moubin Lin[3]†, Beizi Xing[1,2], Hongmiao Wang[1,2], Haosong Zhang[1,2], Zimu Cai[4], Xinyu Mei[3]*, Zheng-Jiang Zhu[1,2,5]*

Metabolic dysregulation and altered metabolite concentrations are widely recognized as key characteristics of aging. Comprehensive exploration of endogenous metabolites that drive aging remains insufficient. Here, we conducted an untargeted metabolomics analysis of aging mice, revealing citrulline as a consistently down-regulated metabolite associated with aging. Systematic investigations demonstrated that citrulline exhibited antiaging effects by reducing cellular senescence, protecting against DNA damage, preventing cell cycle arrest, modulating macrophage metabolism, and mitigating inflammaging. Long-term citrulline supplementation in aged mice yielded beneficial effects and ameliorated age-associated phenotypes. We further elucidated that citrulline acts as an endogenous metabolite antagonist to inflammation, suppressing proinflammatory responses in macrophages. Mechanistically, citrulline served as a potential inhibitor of mammalian target of rapamycin (mTOR) activation in macrophage and regulated the mTOR–hypoxia-inducible factor 1α–glycolysis signaling pathway to counter inflammation and aging. These findings underscore the significance of citrulline deficiency as a driver of aging, highlighting citrulline supplementation as a promising therapeutic intervention to counteract aging-related changes.

INTRODUCTION

Aging, a prevalent risk factor for numerous chronic diseases in humans, presents a persistent and notable public health challenge (*1*). The intricate relationship between metabolism and aging has garnered extensive attention and investigation, revealing metabolic dysregulation and altered metabolites as key hallmarks of aging (*2*, *3*). However, whether these metabolic changes are consequences of aging or drivers of the aging process remains largely unexplored. Aging-associated metabolic dysregulations often result in the accumulation or deficiency of certain metabolites (*4*, *5*). For instance, the metabolite trimethylamine N-oxide (TMAO) has been found to accumulate in human blood with aging and is associated with detrimental effects (*6*). High concentrations of TMAO are linked to an increased risk of cardiovascular disease and all-cause mortality (*7*, *8*). In contrast, nicotinamide adenine dinucleotide (NAD) has emerged as a prominent example of an aging hallmark metabolite (*9*–*11*). Supplementation with NAD precursors, such as nicotinamide mononucleotide (NMN), has shown promise as a strategy for protecting against age-associated diseases and potentially extending health span and life span (*12*, *13*). Recently, Singh *et al.* (*14*) highlighted taurine deficiency as a contributor to aging, and taurine supplementation has demonstrated potential in slowing down key markers of aging. Another noteworthy example is spermidine, extensively studied for its ability to enhance longevity in various animal models (*15*). Dietary intake of spermidine from nutrients has been found to correlate with reduced cardiovascular and cancer-related mortality in human epidemiological studies (*16*). Numerous studies have shown that changes in endogenous metabolites exhibit remarkable conservation across different species (*17*). Therefore, understanding the role of metabolites in aging is crucial for unraveling the mechanisms underlying age-related diseases, developing effective interventions, and promoting healthy aging. However, the comprehensive exploration of endogenous metabolites that drive the aging process remains insufficient.

Aging is characterized by chronic inflammation, commonly referred to as inflammaging, which manifests as a low-grade, persistent proinflammatory state (*18*). Inflammaging plays a pivotal role in tissue dysfunction and the development of age-related pathologies, and it has emerged as a biomarker for accelerated aging (*19*). Traditional inflammation intervention strategies, such as anticytokine therapy and immune cell depletion, may have serious safety concerns and limited applicability in extending human life span. Alternatively, metabolic intervention to suppress inflammaging has shown promising effects in extending both health span and life span. In particular, metabolite supplementation through daily nutrition has become prevalent intervention to modulate inflammaging and counter aging. For example, spermidine supplement has been shown to enhance immune function, resulting in the delay of age-related pathologies in various organisms (*15*, *20*). In addition, supplementation with the endogenous metabolite α-ketoglutarate has been demonstrated to extend lifespan and compress morbidity in aging mice by counteracting inflammatory processes (*21*). These findings highlighted that targeting inflammaging serves as a potential strategy to counteract aging.

The immune system undergoes a progressive decline as aging (*22*). This decline is attributed to age-related changes in macrophages, which are major contributors to age-associated inflammation (i.e., inflammaging) (*23*). Macrophages play a crucial role in initiating inflammatory responses against pathogens and facilitating tissue repair, adapting their function based on local cytokine signals to promote either proinflammatory or anti-inflammatory responses (*24*, *25*). However, aging leads to phenotypic and functional changes in macrophages, affecting processes such as phagocytosis, wound healing, and polarization (*26*, *27*). Dysregulation of anti-inflammatory function of

[1]Interdisciplinary Research Center on Biology and Chemistry, Shanghai Institute of Organic Chemistry, Chinese Academy of Sciences, Shanghai 200032, P. R. China. [2]University of Chinese Academy of Sciences, Beijing 100049, P. R. China. [3]Center for Clinical Research and Translational Medicine, Yangpu Hospital, Tongji University School of Medicine, Shanghai 200090, P.R. China. [4]College of Marine Life Sciences, Ocean University of China, Qingdao 266003, P. R. China. [5]Shanghai Key Laboratory of Aging Studies, Shanghai 201210, P. R. China.
*Corresponding author. Email: jiangzhu@sioc.ac.cn (Z.-J.Z.); meixy@tongji.edu.cn (X.M.)
†These authors contributed equally to this work.

macrophages has been proposed as a contributing factor to the increased susceptibility of the elderly people to sepsis and inflammatory disorders (*28*). Previous study has demonstrated that metabolic shifts during aging, including alterations in oxidative phosphorylation, glycolysis, and urea cycle, play regulatory roles in macrophage-mediated inflammatory responses (*23*, *29*). These aging-related metabolic shifts mediate pathogen clearance and tissue repair and increase susceptibility to infections and age-related inflammatory diseases (*30*). Thus, the age-related impairment of macrophage metabolism, particularly the loss of anti-inflammatory capacity, serves as a potential target for countering aging.

In this study, we used liquid chromatography–mass spectrometry (LC-MS)–based untargeted metabolomics to comprehensively analyze endogenous metabolites in various organs of aging mice. We observed the consistent down-regulation of citrulline with aging. Further results demonstrated that citrulline supplementation effectively reduced cellular senescence, protected against DNA damage, prevented cell cycle arrest, and mitigated inflammaging and other age-related phenotypes in various cell and mouse models. Notably, long-term citrulline supplementation in aged mice yielded beneficial effects, ameliorating age-associated phenotypes and extending health span. Comprehensive mechanistic investigations established that citrulline acts as an endogenous metabolite antagonist to inflammation and enables to suppress proinflammatory responses through mediating the mammalian target of rapamycin (mTOR)–hypoxia-inducible factor 1α (HIF1α)–glycolysis signaling pathway in macrophages to counter aging. These findings underscore the critical role of citrulline deficiency as a driver of the aging process and highlight citrulline supplementation as a potential therapeutic intervention to counteract aging-related changes.

RESULTS

Citrulline is significantly down-regulated during aging

Metabolic dysregulation is widely acknowledged as one of the key characteristics of aging. To explore the role of metabolism in the aging process, we conducted a comprehensive analysis of metabolic changes in brain tissue, liver tissue, and serum samples from male mice at different ages (6, 24, 36, 52, and 78 weeks old). LC-MS–based untargeted metabolomics was used. By applying the Kruskal-Wallis test and Spearman correlation, we identified 75, 106, and 80 age-associated metabolites in the brain, liver, and serum, respectively (Fig. 1A and fig. S1, A and B). Metabolic pathway enrichment analysis of age-associated metabolites revealed significant enrichment primarily in purine metabolism, pyrimidine metabolism, and five other pathways in mouse brain tissue, while purine metabolism, pyrimidine metabolism, amino sugar and nucleotide sugar metabolism, pyruvate metabolism, and nine other pathways were enriched in mouse liver tissue (Fig. 1B). Furthermore, mouse serum exhibited enrichment in the cysteine and methionine metabolism pathway, phenylalanine metabolism, nicotinate and nicotinamide metabolism, and β-alanine metabolism pathway (Fig. 1B). Further analysis of all age-associated metabolites in mouse brain tissues, liver tissues, and serum identified seven metabolites consistently associated with aging across all three sample groups (Fig. 1, C and D). These metabolites included 1,5-anhydroglucitol, citrulline, cyclamic acid, TMAO, ergothioneine, anserine, and homocitrulline (Fig. 1E and fig. S1C). Previous studies have already linked 1,5-anhydroglucitol (*31*), ergothioneine (*32*), TMAO (*6*, *8*), and homocitrulline (*33*) to aging. Notably, our findings revealed specific down-regulation of citrulline, along with 1,5-anhydroglucitol, in all three sample types (Fig. 1F). In particular, in mouse liver tissue, as early as 24 weeks, the level of citrulline decreased by ~50% compared to that at 6 weeks. Citrulline levels decreased by ~20% during aging in mouse brain and serum. Collectively, these findings highlight the identification of citrulline as a consistently down-regulated metabolite associated with aging in mice.

Citrulline supplementation mitigates age-associated phenotypes in vitro and ex vivo

To investigate the biological function of citrulline in the context of aging, we used a reactive oxygen species–induced cell senescence model for preliminary exploration (*34*). First, we demonstrated that levels of citrulline were dose-dependently decreased in senescent mouse embryonic fibroblast (MEF) cells upon the addition of *tert*-butyl hydroperoxide (tBHP), a reactive oxygen species inducer (Fig. 2A). These results validated the citrulline deficiency observed in aging mice and confirmed the relevance of the senescent MEF cell model. Significantly, we further demonstrated that treatment with citrulline (500 μM) during passage of senescent MEF cells led to a notable reduction in the levels of γ–H2A histone family member X (γH2AX), a molecular marker associated with DNA damage and repair (Fig. 2B). This finding indicated that elevated levels of citrulline contributed to a decrease in DNA damage in senescent cells. Furthermore, citrulline supplementation exhibited a significant inhibition of senescence-associated β-galactosidase (SA-β-Gal) activity (Fig. 2C and fig. S2A). Aging is associated with a decline in cell division capacity, leading to cellular senescence characterized by irreversible growth arrest, including increased expression of senescence markers such as *p21*. Our study suggests that citrulline supplementation attenuates the senescence phenotype by decreasing the expression of *p21* (Fig. 2D). This intervention could potentially delay the onset of senescence and improve cell division capacity in MEFs. In addition to cellular markers, we assessed the impact of citrulline supplementation on the senescence-associated secretory phenotype, characterized by the secretion of high levels of inflammatory cytokines. Our findings revealed that citrulline supplementation effectively reduced the mRNA levels of inflammatory cytokines, including *Tnf*, *Il6*, and *Il1b*, in senescent MEF cells, but not normal ones (Fig. 2E).

Furthermore, we extended our investigation to primary bone marrow–derived macrophages (BMDMs) obtained from both young and aged mice (6 and 78 weeks old, male) to further explore the role of citrulline ex vivo. Consistently, intracellular levels of citrulline were found to be significantly down-regulated in aged BMDMs compared to young BMDMs (Fig. 2F), providing additional validation of its relevance in the context of aging mice. Consistent with the results obtained from senescent MEF cells, we observed that citrulline supplementation in aged BMDM cells effectively attenuated age-associated phenotypes. This was demonstrated by the reduction in the DNA damage marker γH2AX, the inhibition of SA-β-Gal activity, the decrease in mRNA levels of inflammatory cytokines such as *Tnf*, *Il6*, and *Il1b*, and the cell cycle arrest marker *p16*, *p19*, and *p21* (Fig. 2, G to I, and fig. S2, B and C). Notably, these effects were not observed in young BMDM cells, further emphasizing the specific impact of citrulline in the context of aging. We also treated peripheral blood mononuclear cell (PBMC)–derived human macrophages with or without citrulline. Similar to BMDMs derived from mice, we observed that citrulline supplementation in aged human macrophages attenuated the mRNA levels of inflammatory cytokines, including

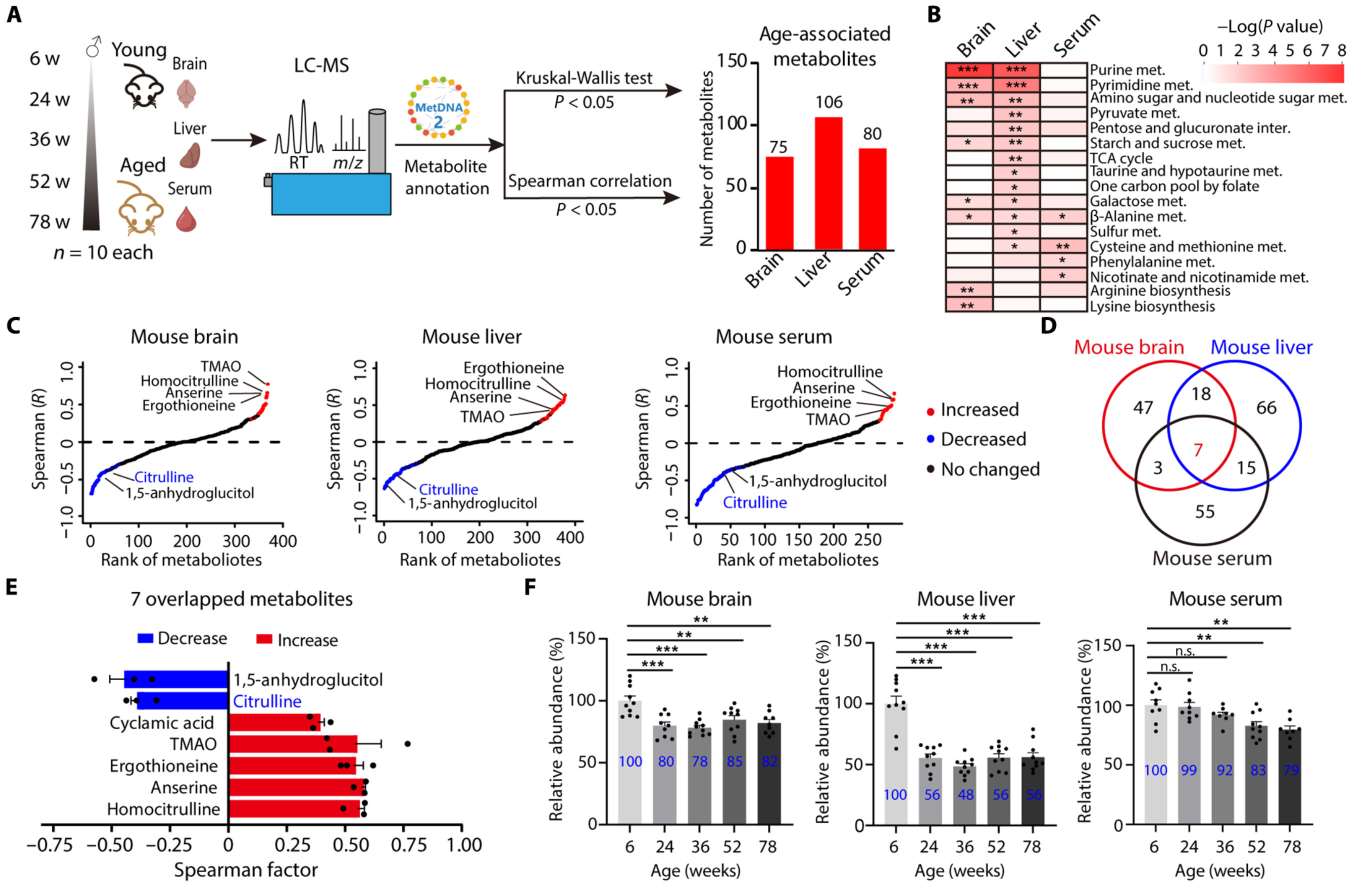

Fig. 1. Citrulline is significantly down-regulated during aging. (**A**) Graphic illustration of the workflow to profile age-associated metabolites in brain tissue, liver tissue and serum from mice at different ages using LC-MS. Age-associated metabolites were screened by Kruskal-Wallis test ($P < 0.05$) and Spearman correlation ($P < 0.05$). w, weeks; *m/z*, mass/charge ratio. (**B**) Pathway enrichment analyses of age-associated metabolites from mouse brain, liver, and serum (hypergeometric test, $^{***}P < 0.001$, $^{**}P < 0.01$, and $^{*}P < 0.05$). TCA, tricarboxylic acid. (**C**) Age-associated metabolites were screened by Kruskal-Wallis test ($P < 0.05$) and Spearman correlation ($P < 0.05$). Red dots (brain, $n = 26$; liver, $n = 46$; serum, $n = 21$) and blue dots (brain, $n = 49$; liver, $n = 60$; serum, $n = 59$) represent metabolites that were increased and decreased over the age, respectively. Black dots represent unchanged metabolites. (**D**) Venn diagram for the overlap of age-associated metabolites in mouse brain, liver, and serum obtained from (C). (**E**) The spearman factors of seven common age-associated metabolites in mouse brain, liver, and serum datasets. Red and blue bars represent metabolites that were increased and decreased over the age, respectively. $n = 3$. Three dots for each metabolite represent their Spearman factors with age obtained from mouse brain, liver, and serum datasets, respectively. (**F**) Relative abundances of citrulline in mouse brain, liver, and serum at different ages. Bars represent means ± SEM. $n = 8$ to 10; all numbers are biologically independent samples. $^{***}P < 0.001$, $^{**}P < 0.01$, and $^{*}P < 0.05$; n.s., not significant (two-tailed Student's *t* test).

TNF and *IL1B* (Fig. 2J). Collectively, citrulline supplementation demonstrated its ability to mitigate age-associated phenotypes, including DNA damage, senescence markers, and inflammatory cytokine levels, in both in vitro and ex vivo models. These findings underscore the significance of citrulline deficiency as a key driver of the aging process.

Beneficial effects of long-term citrulline supplementation in aged mice

To investigate the biological function of citrulline in vivo in counteracting aging, we conducted a long-term administration of citrulline to both young and aged mice (6 and 72 weeks old, male) via drinking water for ~9 weeks (Fig. 3A). LC-MS analyses clearly demonstrated a significant increase in citrulline levels in aged mouse brain tissue, liver tissue, and BMDMs (fig. S3A). Longitudinal monitoring of mouse body weights revealed a significant decrease in body weights of old mice after ~5 to 6 weeks of citrulline supplementation, while the body weights of young mice remained unaffected (Fig. 3B). To eliminate the contribution of body weight, we further selected and analyzed mice with overlapping body weights between the aged group ($n = 3$) and the aged + citrulline group ($n = 6$) (fig. S3B; $P = 0.63$, two-tailed Student's *t* test). We then compared the mRNA levels of aging-associated inflammatory cytokines in brain and liver tissues. The results showed that citrulline supplementation reduced the mRNA levels of inflammatory cytokines (*Tnf*, *Il6*, and *Il1b*) in these tissues (fig. S3, C and D). Furthermore, organ weights such as the spleen and liver were also reduced in response to 9 weeks of citrulline supplementation exclusively in old mice (Fig. 3C). During aging, the liver and spleen of mice increase in weight primarily due to factors such as fat accumulation (*35*, *36*) and inflammatory responses (*37*). Obesity is often accompanied by a low-grade chronic inflammatory state (*38*). In light of this, anti-inflammatory nutrition has emerged as a pharmacological approach to treating obesity (*39*). We hypothesize that citrulline supplementation may prevent the increase in spleen and liver weight by inhibiting

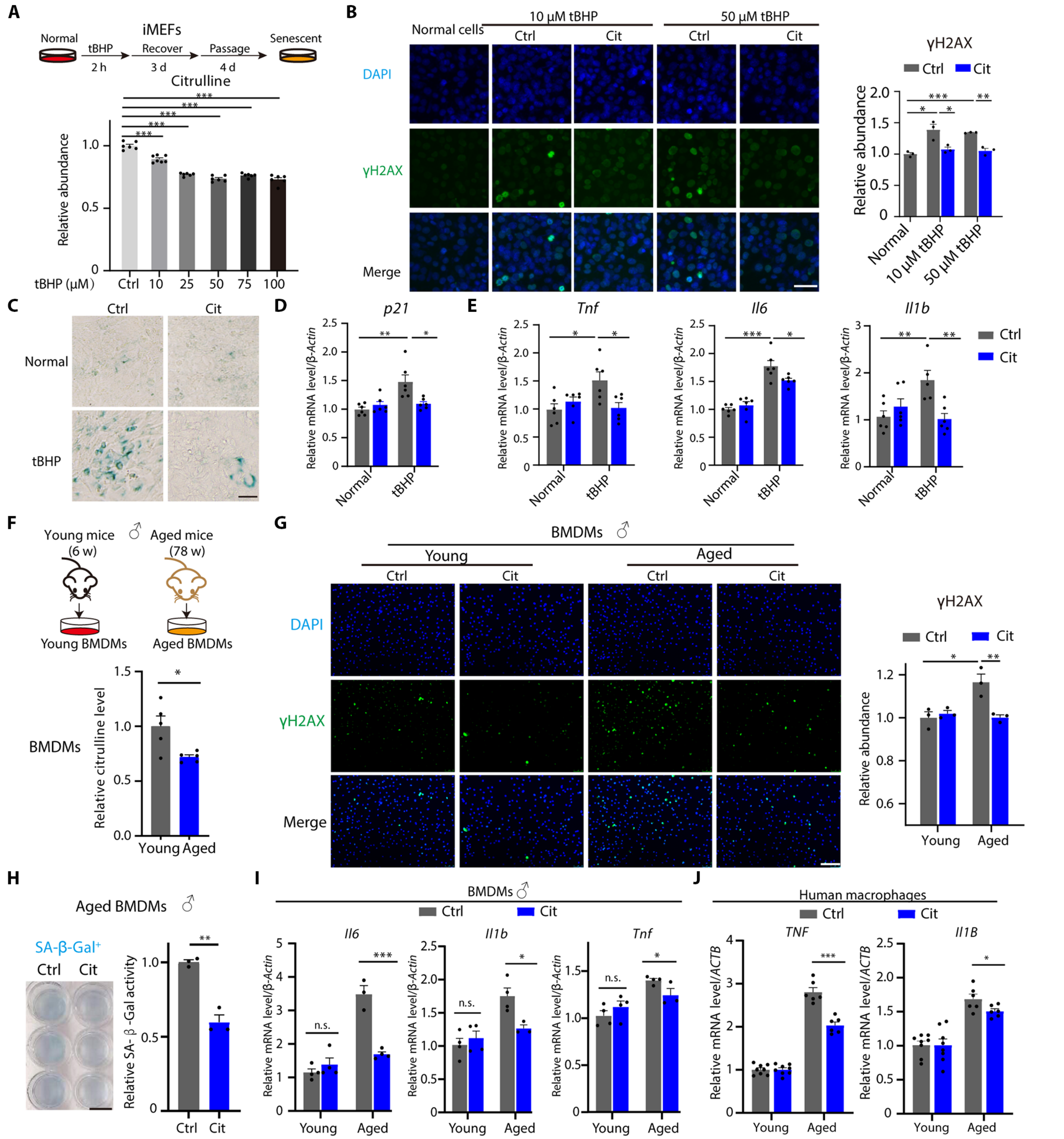

Fig. 2. Citrulline supplement mitigates age-associated phenotypes in vitro and ex vivo. (**A**) Schematic illustration of senescent immortalized MEF (iMEF) generation using tBHP. $n = 6$ to 7. h, hours; d, days. (**B**) Representative images illustrating γH2AX (green) levels responding to citrulline (Cit; 500 μM for 4 days) in iMEFs with 4′,6-diamidino-2-phenylindole (DAPI)–stained nuclei (blue). $n = 3$; each point averaged from 3 images. Scale bar, 50 μm. (**C**) Representative SA-β-Gal activity staining images in iMEFs responding to citrulline (500 μM for 4 days). Scale bar, 50 μm. (**D**) *p21* mRNA levels in iMEFs responding to citrulline (500 μM for 4 days). $n = 6$. (**E**) mRNA levels of *Tnf*, *Il6*, and *Il1b* in iMEFs responding to citrulline (500 μM for 4 days). $n = 5$ to 6. (**F**) Graphical illustration of BMDM generation and citrulline levels in BMDMs. $n = 5$. (**G**) Representative images illustrating γH2AX (green) levels responding to citrulline (500 μM for 24 hours) in BMDMs with DAPI-stained nuclei (blue). $n = 3$; each point averaged from three images. Scale bar, 100 μm. (**H**) Representative SA-β-Gal activity images in aged BMDM cells after citrulline treatment (500 μM for 24 hours). $n = 3$. Scale bar, 10 mm. (**I**) mRNA levels of *Tnf*, *Il6*, and *Il1b* in BMDMs after citrulline treatment (500 μM for 24 hours). $n = 3$ to 4. (**J**) mRNA levels of *TNF* and *IL1B* in young (19 years old, male) and aged (56 years old, male) human macrophages after citrulline treatment (500 μM for 12 hours). $n = 6$ to 8. Bars represent means ± SEM. $***P < 0.001$, $**P < 0.01$, and $*P < 0.05$ (two-tailed Student's *t* test).

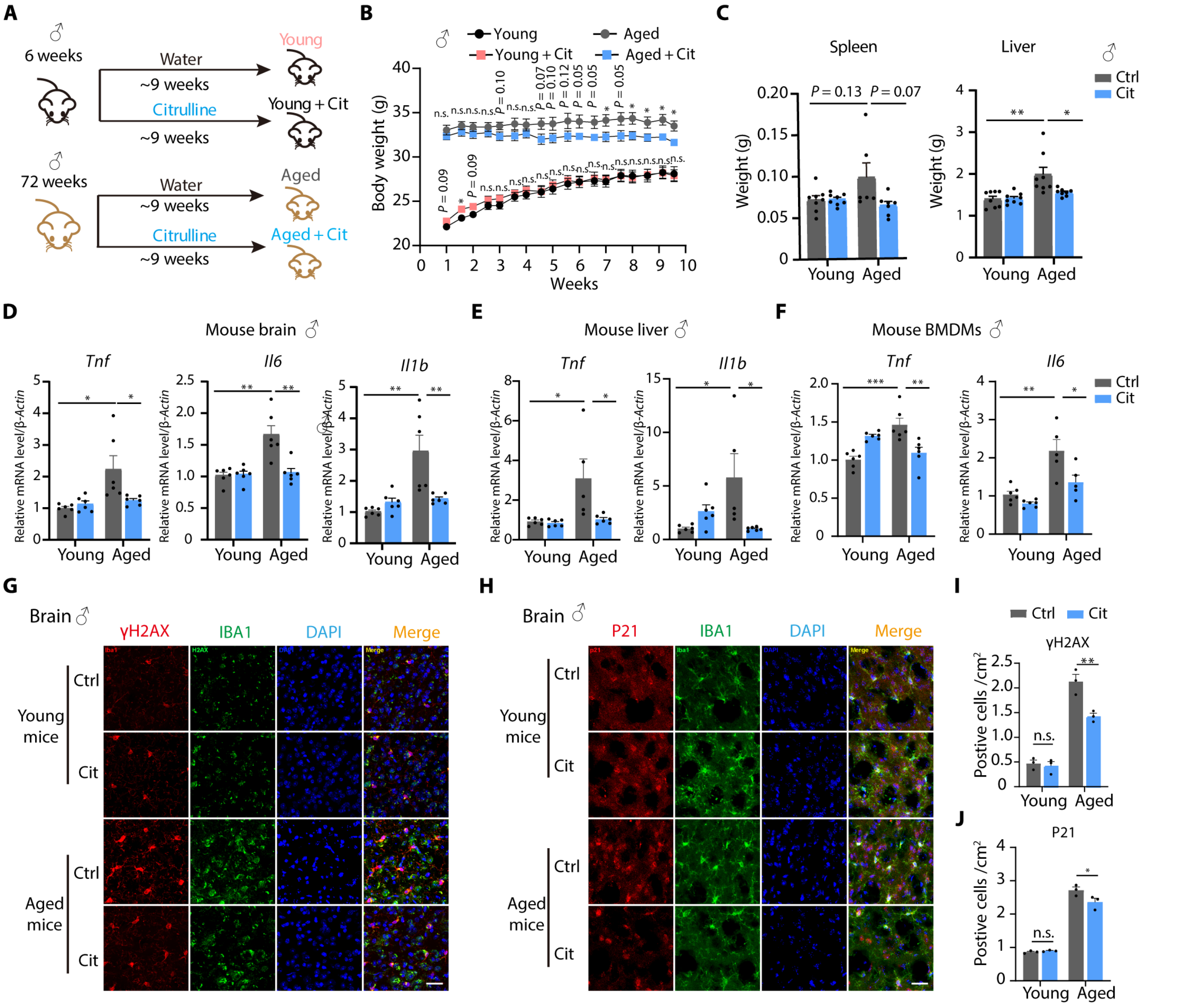

Fig. 3. Beneficial effects of long-term citrulline supplementation in aging mice. (**A**) The long-term supplementation scheme of young and aged mice (male) with drinking water only or drinking waters containing citrulline (1 g/kg of body weight of mice) for about 9 weeks (6 and 72 weeks old, male). $n = 8$. (**B**) Recorded body weights of young and aged mice (male) supplemented with water or citrulline over 9 weeks. $n = 8$. (**C**) Weights of spleen and liver organs in young and aged mice (male) supplemented with water or citrulline over 9 weeks. $n = 6$ to 8. (**D** to **F**) Real-time polymerase chain reaction (PCR) analyses of senescence-associated secretory phenotype genes, including *Tnf*, *Il6*, and *Il1b* in mouse brain (D), liver (E) and primary BMDMs (F). $n = 5$ to 6. (**G** and **H**) Representative immunofluorescence images of γH2AX (G) and P21 (H) levels in brain tissues of young and aged mice (male) supplemented with water or citrulline over 9 weeks. The microglia in the brain were stained with anti-IBA1 antibody (green), and the nuclei were stained with DAPI (blue). Scale bars, 50 μm. (**I** and **J**) The averaged density of positive cells in images from (G) and (H). $n = 3$; each point represents the mean densities of three images in each sample. Bars represent means ± SEM. ***$P < 0.001$, **$P < 0.01$, and *$P < 0.05$ (two-tailed Student's t test).

inflammation during aging. Moreover, we assessed the ability of long-term citrulline supplementation to alleviate age-associated phenotypes in mice. Citrulline supplementation significantly decreased the mRNA levels of aging-associated inflammatory cytokines (*Tnf*, *Il6*, and *Il1b*) in the whole-brain tissues, whole-liver tissues, and primary BMDMs of old mice (Fig. 3, D to F). Microglia, which are tissue-specific macrophages in the brain, have been reported to be activated during aging, resulting in a notable increase in the expression of specific markers such as ionized calcium binding adaptor molecule 1 (IBA1). Our research findings suggest that citrulline inhibits the activation of microglia in aged brain tissues (Fig. 3, G and H). Immunofluorescence staining of γH2AX in brain tissues further confirmed a substantial reduction in age-induced DNA damage following citrulline administration (Fig. 3, G and I). These findings were also supported by immunofluorescence staining of P21 and P16, markers of cell cycle arrest associated with aging (Fig. 3, H and J, and fig. S3, E and F). Notably, these effects of citrulline supplementation were not observed in young mice, providing additional evidence that citrulline deficiency is a key driver of aging. Overall, long-term supplementation of citrulline to aged mice resulted in increased endogenous citrulline levels and effectively reduced body weights, as well as spleen and liver weights, along with other age-associated phenotypes. These results demonstrate the potential of citrulline as a therapeutic intervention to counteract aging-related changes.

Citrulline is an endogenous metabolite antagonist to inflammation

While previous studies have established the role of citrulline in modulating inflammation, its function in the context of aging has yet to be explored. To address this, we first conducted experiments to validate the anti-inflammatory function of citrulline. Our findings from LC-MS analysis revealed that lipopolysaccharide (LPS) treatment significantly increased endogenous citrulline levels in various macrophages, including immortalized BMDM (iBMDM), BV2, and RAW264.7 cells (fig. S4, A to G). Notably, citrulline supplementation effectively reduced the mRNA expressions of inflammatory cytokines (*Tnf*, *Il6*, and *Il1b*) and secretory proteins [tumor necrosis factor–α (TNFα) and interleukin-6 (IL-6)] in LPS-treated iBMDMs (Fig. 4, A and B). Similar results were observed in BV2 and RAW264.7 cells (fig. S4, H to K). These results strongly support the notion that citrulline acts as an endogenous metabolite antagonist to inflammation.

Furthermore, we sought to validate the anti-inflammatory effects of citrulline in mouse models (Fig. 4C). In an LPS-induced acute liver injury model, mice administered LPS and galactosamine (GalN) experienced fatal liver injury within 8 hours (Fig. 4D). However, citrulline administration significantly prolonged the survival time of mice with acute liver injury ($P = 0.003$). Similarly, in a sepsis model where mice were exposed to a lethal dose of LPS (35 mg/kg of body weight), citrulline administration also extended the survival time of septic mice ($P = 0.0176$; Fig. 4E). To further confirm the antagonist role of citrulline in inflammation, we administered mice a nonlethal low dose of LPS (20 mg/kg of body weight) and measured the levels of inflammatory cytokines. Our results demonstrated that in the context of LPS-induced inflammation, citrulline levels were up-regulated in mouse liver tissues but down-regulated in mouse serum (Fig. 4F). Supplementation of citrulline increased the endogenous levels of citrulline in both the liver and serum of mice. Increased endogenous citrulline inhibited the expressions of *Il6* and *Il1b* in mouse liver and reduced the protein levels of IL-6 and IL-1β in mouse serum, while having no significant effects on TNFα (Fig. 4, G and H, and fig. S4L). We found citrulline also influenced the inflammasome, indicating by inhibiting the IL-1β release to the medium in iBMDMs (fig. S4M). These in vitro findings align with the observed effects in the in vivo model, particularly on IL-1β release. These findings provide further evidence for the antagonist role of citrulline in inflammation.

Then, we extended our investigation to determine whether the anti-inflammatory effect of citrulline remains functional in the context of aging. To achieve this, we used primary BMDMs obtained from both young and aged mice (6 and 78 weeks old, male). Consistently, LPS treatment significantly increased the endogenous levels of citrulline in both young and aged BMDMs, albeit to a slightly lesser extent in aged BMDMs (Fig. 4I). To assess the impact of citrulline on age-associated inflammation, we measured the levels of inflammatory cytokines. LPS-induced inflammation was significantly heightened in aged BMDMs; however, supplementation with citrulline effectively reduced the mRNA expressions of age-associated inflammatory cytokines (*Tnf*, *Il6*, and *Il1b*) exclusively in LPS-induced aged BMDMs, while no significant effect was observed in young BMDMs (Fig. 4J). Consistently, citrulline supplementation successfully rescued the activity of SA-β-Gal in LPS-treated aged BMDMs (Fig. 4K and fig. S4N). We also detected the mRNA expressions of age-associated inflammatory cytokines in PBMC-derived human macrophages. Similar to mouse macrophages, citrulline down-regulated the mRNA expressions of *TNF*, *IL6*, and *IL1B* exclusively in LPS-treated aged human macrophages, while no significant effect was detected in young human macrophages (Fig. 4, L and M). These findings provide compelling evidence that citrulline acts as an endogenous metabolite antagonist to inflammation, thereby serving as a potential approach to counteract aging.

Citrulline modulates macrophage metabolism to counter aging and inflammation

To further investigate the regulatory mechanism of citrulline in aging and inflammation, we treated young and aged primary BMDMs with or without citrulline and subjected to comprehensive untargeted metabolomics profiling (Fig. 5A). A total of 192 metabolites were altered between young and aged BMDMs, and citrulline supplementation rescued 102 of these metabolites (fig. S5, A and B). Principal components analysis (PCA) revealed that age-associated metabolic alterations in BMDMs were partially rescued upon citrulline treatment, particularly in PC1 dimension (Fig. 5A). Metabolic pathway enrichment analysis further showed that metabolic activity of aged BMDMs was up-regulated compared to young BMDMs, but this increase was attenuated in aged BMDMs with citrulline treatment (Fig. 5B). In particular, age-induced up-regulation of glycolysis and gluconeogenesis pathway in BMDMs, which is an important energy metabolism pathway, was partially diminished by citrulline supplementation. Therefore, we propose that citrulline might exert its antiaging and anti-inflammation effects through influencing the glycolysis pathway. Furthermore, our data validated that citrulline supplementation rescued aging-induced expressions of glycolysis genes encoding *Hk2* (hexokinase 2), *Pkm2* (pyruvate kinase muscle isozyme M2), *Pgk1* (phosphoglycerate kinase 1), *Pgam1* (phosphoglycerate mutase 1), *Pfkl* (phosphofructokinase, liver type), *Eno1* (enolase 1), *Gpi* (glucose-6-phosphate isomerase), and *Ldha* (lactate dehydrogenase A), as well as glycolysis metabolites, including fructose 6-phosphate, pyruvate, and lactate in aged BMDMs (Fig. 5C and fig. S5C). Since mTOR and HIF1α signaling pathway was well reported to regulate glycolysis and had close associations with aging and inflammation, we further demonstrated that increased mRNA and protein expressions of HIF1α in aged BMDMs were also rescued by citrulline treatment (Fig. 5D). Consistently, we observed that the activation of mTOR in aged BMDMs was also rescued by citrulline supplemention through measuring phosphorylation of mTOR phosphorylation (mTOR; Ser^{2448}) and its downstream substrates p70S6 kinase (p70S6k; Thr^{389}) and 4E-binding protein 1 (4EBP1; $Thr^{37/46}$) (Fig. 5E). These results suggested that citrulline may modulate macrophage metabolism and regulate mTOR-HIF1α-glycolysis signaling pathway to counter aging (Fig. 5F).

We further demonstrated the regulatory role of citrulline in the context of inflammation by modulating mTOR-HIF1α-glycolysis pathway. Treatment with citrulline reduced the LPS-induced elevation of phosphorylated mTOR, p70S6k, and 4EBP1 in iBMDM cells (Fig. 5G). Consequently, increased mRNA level and protein level of HIF1α responding to LPS induction were also rescued by citrulline supplementation in iBMDMs (Fig. 5H). Measurements of mRNA expressions of glycolysis genes, including *Pfkl*, *Pgk1*, *Tpi*, *Pkm2*, *Gpi*, *Pgam1*, *Ldha*, *Hk2*, *Gapdh*, *Eno1*, and *Aldoa*, and extracellular acidification rates (ECARs) showed citrulline supplementation decreased LPS-induced up-regulation of glycolysis activity in iBMDM cells (Fig. 5, I and J, and fig. S5D). Consistently, LPS-induced up-regulations of glycolysis metabolites, including dihydroxyacetone phosphate, phosphoenolpyruvate, fructose 1,6-bisphosphate, glucose 1,6-bisphosphate, and lactate,

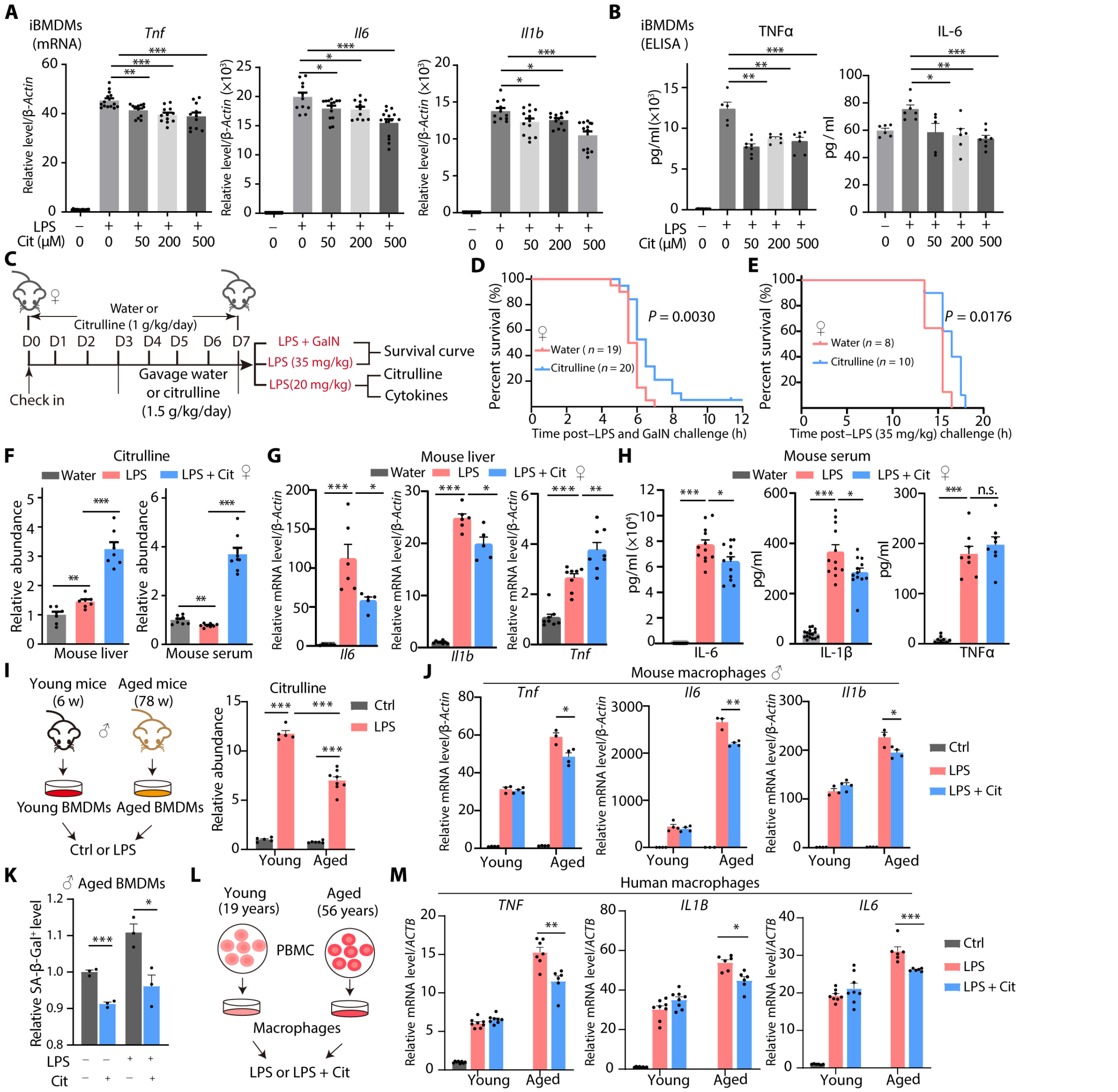

Fig. 4. Citrulline is an endogenous metabolite antagonist to inflammation. (**A**) *Tnf*, *Il6*, and *Il1b* levels in iBMDMs responding to citrulline (4.5 hours) and LPS (100 ng/ml for 4 hours). $n = 12$, three samples with four technical replicates. (**B**) TNFα and IL-6 levels in iBMDM culture medium responding to citrulline (4.5 hours) and LPS (100 ng/ml for 4 hours). $n = 5$ to 8. (**C**) The scheme of mice administrated for 7 days. (**D** and **E**) Mouse survival after LPS challenge using log-rank (Mantel-Cox) test. (**F**) Citrulline levels in mice treated with citrulline and LPS (20 mg/kg). $n = 8$. (**G**) *Tnf*, *Il6*, and *Il1b* levels in mouse liver treated with citrulline and LPS (20 mg/kg). $n = 5$ to 8. (**H**) TNFα, IL-6, and IL-1β levels in mouse serum treated with citrulline and LPS (20 mg/kg). $n = 8$ to 16. (**I**) Graphical illustration of BMDM generation and citrulline levels in BMDMs treated with LPS (100 ng/ml for 12 hours). $n = 5$ or 8. (**J**) *Tnf*, *Il6*, and *Il1b* levels in BMDMs responding to citrulline (500 μM for 12.5 hours) and LPS (100 ng/ml for 12 hours). $n = 3$ to 4. (**K**) Quantifications of SA-β-Gal activities in BMDMs responding to citrulline (500 μM for 12.5 hours) and/or LPS (100 ng/ml for 12 hours). $n = 3$. (**L**) Graphical illustration of human macrophages from PBMCs. (**M**) *TNF*, *IL1B*, and *IL6* levels responding to citrulline (500 μM for 12.5 hours) and LPS (100 ng/ml for 12 hours) in human macrophages. $n = 6$ to 8. Bars represent means ± SEM. $^{***}P < 0.001$, $^{**}P < 0.01$, and $^{*}P < 0.05$ (two-tailed Student's *t* test).

were also rescued by citrulline treatment (fig. S5E). Oxygen consumption rate (OCR) analysis showed the addition of citrulline significantly increased LPS-induced adenosine 5′-triphosphate (ATP) production in iBMDM cells (fig. S5F).

We further confirmed that citrulline exerts its anti-inflammatory effects through the suppression of the mTOR-HIF1α-glycolysis pathway under both reduced and elevated citrulline conditions. We first used L-NG-nitroarginine methyl ester (L-NAME), a widely used inhibitor of nitric oxide synthase 2 (NOS2) (40), to create a citrulline-depleted environment. Consistently, our results showed that L-NAME treatment reduced citrulline levels in a dose-dependent manner (fig. S5G). Accordingly, Western blot results revealed that the LPS-induced

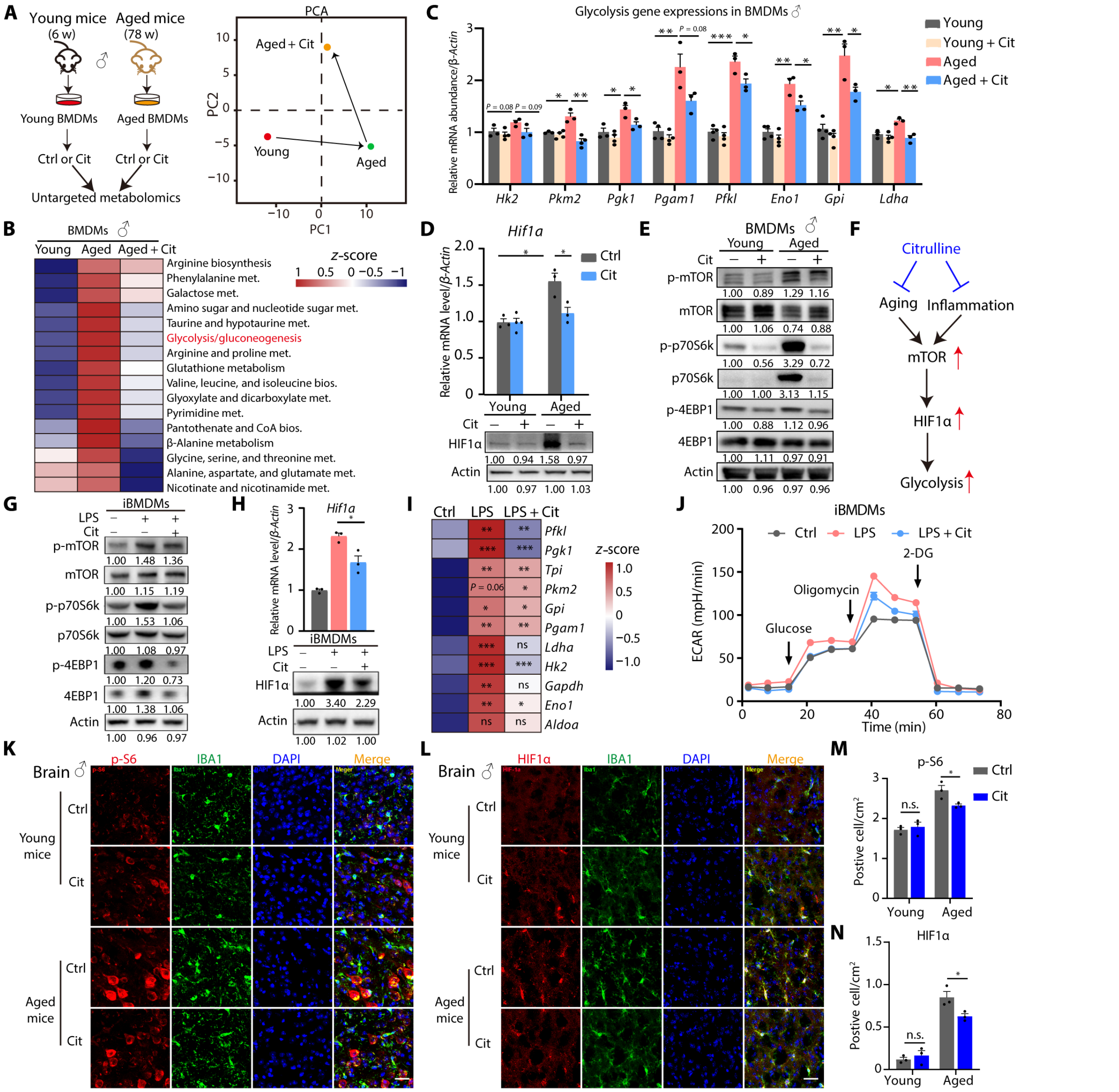

Fig. 5. Citrulline modulates macrophage metabolism to counter aging and inflammation. (**A**) BMDMs from mice were treated with citrulline (500 μM for 12 hours) for untargeted metabolomics. (**B**) Sixteen enriched metabolic pathways in aged BMDMs treated with citrulline (500 μM for 12 hours). CoA, coenzyme A. (**C**) Glycolysis gene levels in BMDMs treated with citrulline (500 μM for 12 hours). $n = 3$ to 4. (**D**) HIF1α expressions in BMDMs treated with citrulline (500 μM for 12 hours). $n = 3$ to 4. (**E**) p-mTOR, mTOR, p-p70S6k, p70S6k, p-4EBP1, and 4EBP1 expressions in BMDMs responding to citrulline (500 μM for 12 hours). (**F**) A proposed model for citrulline to counter aging and inflammation through modulating mTOR-HIF1α-glycolysis. (**G**) p-mTOR, mTOR, p-p70S6k, p70S6k, p-4EBP1, and 4EBP1 expressions r4esponding to citrulline (500 μM for 4.5 hours) and LPS (100 ng/ml for 4 hours) in iBMDMs. (**H**) HIF1α expressions in iBMDMs treated with citrulline (500 μM for 4.5 hours) and LPS (100 ng/ml for 4 hours). $n = 3$. (**I**) Glycolysis genes in iBMDMs treated with citrulline (500 μM for 4.5 hours) and LPS (100 ng/ml for 4 hours). $n = 3$. (**J**) ECAR of iBMDMs treated with citrulline (500 μM for 4.5 hours) and LPS (100 ng/ml for 4 hours). $n = 6$ to 11. (**K** and **L**) Representative images of p-S6 (K) and HIF1α (L) in mouse brain. Microglia were stained with anti-IBA1 antibody (green) and DAPI (blue). Scale bars, 50 μm. (**M** and **N**) Averaged density of positive cells in (K) and (L). $n = 3$; each point represents the mean from three images. Bars represent means ± SEM. $^{***}P < 0.001$, $^{**}P < 0.01$, and $^{*}P < 0.05$ (two-tailed Student's t test).

activation of the mTOR pathway was enhanced in response to L-NAME treatment (fig. S5H). Furthermore, citrulline supplementation effectively suppressed mTOR activation in L-NAME–inhibited iBMDMs (fig. S5I). Consistently, in L-NAME–inhibited iBMDMs, we observed that the mTOR inhibitor rapamycin significantly decreased the mRNA expression of LPS-induced proinflammatory cytokines, including *Tnf*, *Il6*, and *Il1b* (fig. S5J). In addition, we found that L-NAME treatment decreased citrulline levels without influencing arginine levels, indicating that the anti-inflammatory effect was independent of arginine (fig. S5K). We also used α-methyl-DL-aspartic acid, a specific argininosuccinate synthase 1 (ASS1) inhibitor (*41*), to induce citrulline accumulation. Western blot results indicated that the LPS-induced activation of the mTOR pathway was inhibited in response to α-methyl-DL-aspartic acid treatment (fig. S5L). Furthermore, under citrulline supplementation condition, we used the mTOR agonist MHY1485 or the HIF1α stabilizer dimethyloxalylglycine to promote mTOR activation or HIF1α stabilization, respectively. These treatments resulted in increased HIF1α protein levels (fig. S5M) and elevated mRNA and protein levels of the proinflammatory cytokine TNFα (fig. S5, N and O).

Immunofluorescence staining of p-S6 (an in vivo marker for mTOR activity) and HIF1α in brain tissues from aged mice confirmed significant reductions in age-induced activations of mTOR and HIF1α after long-term administration of citrulline over 9 weeks (Fig. 5, K to N).These results demonstrated that citrulline supplementation rescued age-associated metabolic alterations and modulated the mTOR-HIF1α-glycolysis pathway in BMDMs, indicating its regulatory role in macrophage metabolism to counter aging and inflammation.

Age-dependent down-regulation of *Nos2* contributed to citrulline deficiency in macrophages

We identified the deficiency of citrulline during the aging process; however, the factors contributing to this deficiency remain unknown. To investigate this further, we used stable-isotope tracing metabolomics technology using [U-^{13}C]-arginine as a tracer (Fig. 6A). We administered 0.4 mM [U-^{13}C]-arginine to both young and old primary BMDMs for 24 hours and measured the ^{13}C-labeled metabolites involved in citrulline metabolism, namely, arginine, ornithine, argininosuccinate, and citrulline. Unexpectedly, there were no significant changes observed in the total levels or ^{13}C-labeled forms of arginine, ornithine, and argininosuccinate between the young and old BMDMs (Fig. 6, B to D). The results were consistent with our untargeted metabolomics data in mice (fig. S6A). However, the M6 isotopologue of citrulline exhibited a significant decrease in old BMDMs (Fig. 6E). Citrulline anabolism involves two pathways. The first pathway involves the conversion of ornithine to citrulline in the mitochondria. In this case, the M6 isotopologue of arginine gives rise to the M5 isotopologue of ornithine, which further generates the M5 isotopologue of citrulline. However, as illustrated in Fig. 6E, no M5 isotopologue of citrulline was detected, suggesting that the conversion of ornithine to citrulline in the mitochondria does not occur in BMDM metabolism. The second pathway entails the direct conversion of arginine to citrulline through NOS2. In this case, the M6 isotopologue of arginine directly forms the M6 isotopologue of citrulline. Consequently, our experiment measured the M6 isotopologue of citrulline, which exhibited a significant decline in aged BMDMs. Furthermore, we assessed the mRNA expression of *Nos2*, which consistently showed

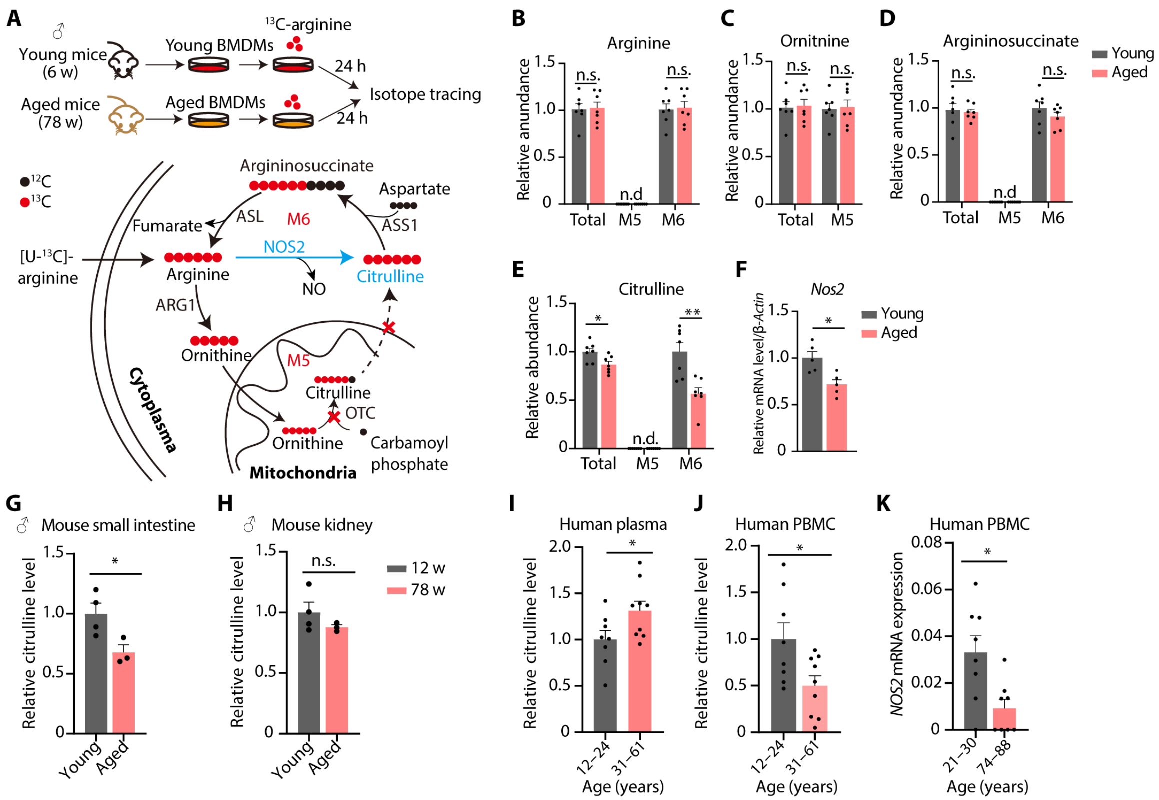

Fig. 6. Age-dependent down-regulation of *Nos2* contributed to citrulline deficiency in macrophages. (**A**) Schematic illustration of stable-isotope tracing metabolomics using [U-^{13}C]-arginine as a tracer. Young and aged BMDMs (male mice) were treated with 0.4 mM [U-^{13}C]-arginine for 24 hours. OTC, ornithine transcarbamylase ; ASL, argininosuccinate lyase. Black dots represent ^{12}C and red dots represent ^{13}C. (**B** to **E**) Relative abundances of metabolites in citrulline metabolism, including arginine (B), ornithine (C), arginosuccinate (D), and citrulline (E), in young and aged BMDMs (male mice) after stable-isotope tracing. $n = 7$ biologically independent samples in each group. n.d., not detected. (**F**) Real-time PCR analyses of *Nos2* mRNA expressions in citrulline metabolism in young and aged BMDMs (male mice) after stable-isotope tracing. Bar graphs represent means ± SEM. $n = 5$. (**G** and **H**) Relative citrulline levels in the small intestine (G) and kidney (H) of young and aged mice (male) determined by LC-MS. $n = 3$ to 4. (**I** to **K**) Relative citrulline levels in plasma and PBMC samples from healthy humans: plasma (I), PBMC (J), and *NOS2* expression from PBMCs (K) in young and aged human. The *NOS2* expressions were derived from the PBMC transcriptome of healthy human donors using RNA sequencing (*42*). Bars represent means ± SEM. $n = 7$ to 9. Bars represent means ± SEM. ***$P < 0.001$, **$P < 0.01$, and *$P < 0.05$ (two-tailed Student's t test).

a decrease in aged BMDMs (Fig. 6F). We conducted similar experiments using tBHP-induced senescent MEF cells (fig. S6, B to F). In these cells, the direct conversion of arginine to citrulline through NOS2 was also significantly reduced, as evidenced by the M6 isotopologue of citrulline (fig. S6F) and *Nos2* mRNA expression (fig. S6G). We observed that the conversion of ornithine to citrulline in the mitochondria occurred in MEF cells, but there were no significant changes observed in the M5 isotopologue of citrulline (fig. S6F). These findings highlight that the deficiency of citrulline during aging can be attributed to the decreased expression of the anabolic enzyme NOS2.

Furthermore, to investigate whether the anti-inflammatory effect of citrulline in macrophages relies on nitric oxide, we used L-NAME to reduce the production of nitric oxide induced by LPS treatment. Our data revealed that the increase in citrulline induced by LPS was diminished following L-NAME treatment (fig. S6H). These results confirmed the successful inhibition of NOS2 by L-NAME. In addition, the analysis of mRNA levels of proinflammatory cytokines, including *Tnf*, *Il6*, and *Il1b*, in response to LPS treatment indicated that inhibiting NOS2 with L-NAME significantly increased inflammation, which could be effectively alleviated by citrulline supplementation (fig. S6I). Hence, the anti-inflammatory effect of citrulline is not contingent on the generation of nitric oxide.

To elucidate the age-related decline in citrulline levels in mice, we also assessed citrulline levels in the small intestine and kidney of mice. Note that citrulline was not present in the mouse diet used in our experiment and citrulline is primarily synthesized by intestinal epithelial cells within the mouse small intestine and subsequently released into the bloodstream. In addition, citrulline can undergo metabolism in the kidney to produce arginine. Our findings in Fig. 6 (G and H) illustrate that, compared to young mice (12 weeks old, male), citrulline levels in the small intestine of aged mice (78 weeks old, male) were significantly diminished. However, citrulline levels in the kidney had no changes during aging. Hence, we deduce that the declined citrulline levels in aged mice primarily stem from reduced biosynthesis within the small intestine. In addition, citrulline levels in primary BMDMs were observed to decrease with aging (Figs. 2F and 6E), possibly due to the reduced citrulline levels in the bloodstream. Furthermore, we provided evidence demonstrating that *Nos2*, specifically expressed mainly in immune cells upon stimulation by proinflammatory cytokines, is significantly down-regulated during aging, thereby contributing to the decreased levels of citrulline in primary BMDMs (Fig. 6F). Therefore, we think that both the decreased circulatory citrulline and impaired biosynthesis of citrulline jointly contribute to citrulline deficiency in aged mouse macrophages.

We also expanded our investigation to include plasma and PBMC samples from healthy individuals, measuring citrulline levels using LC-MS. We found that citrulline levels significantly increased during aging in human plasma (Fig. 6I), and the physiological concentration of citrulline in human plasma is ~40 μM (fig. S6J). In contrast, citrulline levels significantly decreased in PBMC samples from aged individuals (Fig. 6J), and *NOS2* mRNA expressions were also decreased in aged human PBMCs (Fig. 6K) (*42*), aligning with our observations in aged mouse macrophages. Notably, more than ~80% of citrulline released by the intestine is metabolized within the kidney to synthesize arginine (*43*). Previous reports have indicated that the decline in renal function during aging leads to reduced citrulline excretion and citrulline accumulation in the body, ultimately resulting in up-regulated citrulline levels in the elderly population (*44*). In summary, our findings indicate that citrulline levels decreased in PBMCs in aged humans, mirroring observations in aged mouse macrophages.

DISCUSSION

Metabolic dysregulation and altered metabolites are widely recognized as key characteristics of aging (*2*, *4*). Numerous studies have investigated the roles of endogenous metabolites, such as NAD (*9*, *10*), taurine (*14*), spermidine (*15*), and others (*8*, *45*, *46*), as drivers of the aging process. In this study, we conducted a comprehensive analysis of metabolic changes in multiple organs of mice at various ages. Our findings provide the first evidence linking citrulline deficiency to aging. We identified multiple antiaging effects of citrulline, including the reduction of cellular senescence, protection against DNA damage, prevention of cell cycle arrest, modulation of macrophage metabolism, and mitigation of inflammaging. Notably, long-term supplementation of citrulline in aged mice demonstrated significant benefits by alleviating age-associated phenotypes and increasing health span. These findings underscore the critical role of citrulline deficiency as a key driver of the aging process and highlight the potential therapeutic intervention of citrulline supplementation to counteract age-related diseases.

To explore the biological mechanism by which citrulline counteracts aging, we demonstrated that citrulline acts as an endogenous metabolite antagonist to inflammation. Macrophages are primary contributors to age-associated inflammation. Our findings unveil that the decline in endogenous citrulline levels impairs the anti-inflammatory function of macrophages, thereby enhancing susceptibility to inflammatory responses during aging. The anti-inflammatory effect of citrulline has been validated in various mouse models, and its efficacy remains intact even in the context of aging. This observation suggests that the age-dependent deficiency of citrulline, acting as an endogenous antagonist to inflammation, triggers inflammaging and accelerates the aging process. In-depth mechanistic investigations have revealed that citrulline supplementation rescues age-associated metabolic alterations in macrophage metabolism. Specifically, we have demonstrated that citrulline modulates the inflammatory responses by regulating the activities of the mTOR-HIF1α-glycolysis signaling pathway in macrophages. Collectively, these results establish that citrulline governs macrophage metabolism and inflammation as a means to counteract aging.

Our study also underscores the remarkable potential of citrulline as an endogenous metabolite inhibitor of the mTOR pathway in the context of inflammation and aging. mTOR serves as a nutrient sensor that regulates cellular metabolism and is linked to cell proliferation, growth, and survival (*47*, *48*). Extensive research has established the mTOR pathway as a negative regulator of lifespan and aging (*49*, *50*). Pharmacological inhibition of mTOR using small-molecule compounds such as rapamycin has been shown to effectively extend longevity in various animal models, including *Caenorhabditis elegans* (*51*), *Drosophila melanogaster* (*52*), *and Mus musculus* (*53*, *54*). However, the discovery of an endogenous metabolite that inhibits mTOR to counter aging has remained elusive. Arginine, leucine, and *S*-adenosylmethionine (SAM; downstream metabolite of methionine) are the known metabolites that are directly sensed by mTOR components [CASTOR (*55*, *56*), Sestrin (*57*, *58*), and SAMTOR (*59*), respectively]. Restriction of methionine or the three branched-chain amino acids—leucine, isoleucine, and valine—extends lifespan in mice (*60*, *61*), but the roles of these metabolites in regulating aging and mTOR are complicated. Our metabolomics data confirmed that arginine, leucine, SAM, and methionine levels remained unchanged during aging in mice. In our study, we extensively demonstrated that citrulline inhibits the activation of the mTOR pathway in macrophages in both inflammatory and aging contexts. This finding highlights citrulline as a promising endogenous metabolite with the potential to inhibit mTOR signaling. While further mechanistic exploration is needed to fully comprehend how citrulline regulates mTOR activation, our findings present an exciting avenue for investigating the interplay between metabolites, mTOR, and their associations with aging and longevity. In our study, we found that in the context of an inflammatory response, citrulline prominently inhibits the activation of the mTOR pathway. It has been reported that citrulline triggers the mTOR pathway in muscle cells and citrulline supplementation is now under investigation for the treatment of sarcopenia (*62*). However, note that sarcopenia of muscle tissue occurs within a malnutrition context rather than an inflammatory environment. Under these differing physiological circumstances, citrulline may exhibit contrasting effects.

Citrulline, a nonessential amino acid, is naturally synthesized in the liver and intestines of mammals (*63*). It is also present in various foods, including watermelon, cucumber, pumpkin, melons, squashes, and gourds (*64*). Citrulline plays a crucial role in the urea cycle. Its supplementation increases plasma levels of arginine, improving the ammonia recycling process and nitric oxide metabolism (*65*). As a result, citrulline supplementation may be beneficial in situations where nitric oxide is relevant, such as enhancing athletic performance (*66*), promoting vascular health (*67*), and addressing erectile dysfunction (*68*). In our study, we have revealed a function of citrulline, independent of nitric oxide, in mediating mTOR activation and acting as an endogenous metabolite antagonist to inflammation and aging. Therefore, citrulline supplementation holds potential therapeutic value in counteracting age-related diseases. In terms of clinical applications, citrulline supplementation has demonstrated potential benefits in relation to inflammation. Citrulline supplementation decreased inflammatory C-reactive protein and IL-6 in serum of patients from critically ill patients (*69*). In addition, citrulline supplementation also improved glycemic status, TNF-α, and high-sensitivity C-reactive protein in patients with type 2 diabetes (*70*). These studies, combined with our findings, suggest that citrulline supplementation may serve as a promising therapeutic intervention for age-related pathologies.

In our study, we think both the decreased circulatory citrulline and impaired biosynthesis of citrulline jointly contribute to macrophage inflammatory profile. Under inflammatory conditions, reduced citrulline levels in the blood and decreased endogenous citrulline synthesis both lead to diminished inflammation suppression, resulting in a proinflammatory phenotype. Under physiological conditions, macrophages maintain intracellular citrulline levels through their own endogenous biosynthesis. Therefore, a reduction in circulating citrulline levels may not significantly affect the anti-inflammatory function of macrophages. During aging, the down-regulation of citrulline levels due to reduced endogenous synthesis, driven by lower expression of the enzyme NOS2, impairs the anti-inflammatory function of macrophages. Thus, the decline in citrulline levels from endogenous synthesis disrupts normal macrophage function. We propose that the synthesis of intracellular endogenous citrulline is more crucial for the anti-inflammatory function of macrophages under physiological conditions.

In our study, we observed a significant increase in the citrulline level in macrophages upon LPS stimulation, contrasting the findings of Mao *et al.* (*71*). To validate our results, we conducted additional experiments under various conditions (fig. S4, A to G) and conducted a thorough review of existing literature (*72*–*74*). Our findings align with numerous other publications consistently reporting similar conclusions, all of which demonstrate a significant increase in citrulline levels upon LPS stimulation. One of the limitations of our study is exclusive use of male mice as the model to screen age-related metabolites, overlooking the potential contribution of female mice. This decision was primarily driven by the need to minimize the inherent variability associated with cyclical reproductive hormones in female mice. However, focusing solely on male mice, we may have missed valuable insights into how sex-specific factors, such as reproductive hormones, could influence the observed metabolic changes. This limitation underscores the importance of future research endeavors to investigate the metabolic profiles in both male and female mice, allowing for a more comprehensive understanding of age-related metabolic alterations across sexes.

MATERIALS AND METHODS

Cell culture

MEF, iBMDM, BV2, and RAW264.7 cells were cultured in Dulbecco's modified Eagle's medium (DMEM) containing 10% fetal bovine serum (FBS) and antibiotics [penicillin (100 U/ml) and streptomycin (100 μg/ml)]. Mouse BMDMs were isolated from C57BL/6J strain of young and aged mice (6 and 78 weeks old, male) and maintained in 70% fresh DMEM [supplemented with 10% FBS, penicillin (100 U/ml), and streptomycin (100 μg/ml)] and 30% L929 cell culture medium. After 6 days of culture, adherent cells were harvested and plated into new wells for further experiments. PBMCs were isolated from healthy individuals and maintained in fresh RPMI 1640 [supplemented with 10% FBS, penicillin (100 U/ml), and streptomycin (100 μg/ml)] with macrophage colony-stimulating factor (50 ng/ml). After 7 days of culture, adherent cells were harvested and plated into new wells for further experiments.

All cells were cultured at 37°C with 5% CO_2. The iBMDMs exhibit comparable characteristics and functions to primary BMDMs, rendering them convenient for cell biology research.

Western blotting analysis

Protein samples were isolated from respective cells by lysis in radioimmunoprecipitation assay buffer (#89900, Thermo Fisher Scientific). The protein samples were then denatured by boiling in SDS loading buffer (5×). Equal amounts of proteins were resolved by SDS–polyacrylamide gel electrophoresis and then transferred onto a polyvinylidene fluoride membrane. The blots were blocked in 5% bovine serum albumin for 1 hour at room temperature and incubated overnight at 4°C with the respective primary antibodies. The following primary antibodies were used: mouse β-actin (Proteintech, #66009-1-Ig), rabbit p-S6(Ser$^{240/244}$) [Cell Signaling Technology (CST), #5364S], rabbit HIF-1α (CST, #36169T), rabbit p16 (Abcam, #ab211542), rabbit p21 (Abcam, ab188224), mouse Iba1 (Abcam, #ab283342), mouse γH2AX (CST, #80312), rabbit p-mTOR(Ser^{2448}) (Proteintech, #67778-1-lg), mouse mTOR (Proteintech, #66888-1-lg), rabbit 4EBP1 (Proteintech, #60246-1-lg), rabbit p-4EBP1(Thr$^{37/46}$) (CST, #2855T), rabbit p70(S6K) (Proteintech, #14485-1-AP), rabbit p-p70(S6K)(Thr^{389}) (CST, #9234T), rabbit TNFα (Proteintech, #17590-1-AP), and rabbit

IL-1β (CST, 12242S). Horseradish peroxidase (HRP)–conjugated secondary antibodies, including goat HRP-goat anti-rabbit immunoglobulin G (GenScript, A00098) and goat HRP-goat anti-mouse immunoglobulin G (GenScript, A00160), were incubated with blot membrane at room temperature for 1 hour, followed by detecting with ECL Western Blotting Detection Reagent (Thermo Fisher Scientific, 32132).

Mice

Mice (C57BL/6) were group housed in a barrier facility at room temperatures of 20° to 26°C with 40 to 70% humidity and 12-hour light/12-hour dark cycles. All mice received a regular chow diet ad libitum. All animal care and experiments were conducted in accordance with the guidelines and approval of the Institutional Animal Care and Use Committees of Interdisciplinary Research Center on Biology and Chemistry, Shanghai Institute of Organic Chemistry, Chinese Academy of Sciences. The number of experimental protocols approved by the ethical committee of IRCBC (Interdisciplinary Research Center of Biology and Chemistry) is ECSIOC_2023-14. Mice matched for age and sex were used and randomly assigned to experimental groups. Aged mice (6, 24, 36, 52, and 78 weeks old, male) were obtained from animal facility, College of Life Sciences, Xiamen University. Mice were first anesthetized with isoflurane and sacrificed. Then, mouse tissues were dissected and immediately frozen using liquid nitrogen.

Long-term citrulline supplementation

Citrulline solutions were prepared in phosphate-buffered saline (PBS) and sterilized by filtration through a 0.22-μm filter (Millipore). Mice (6 and 72 weeks old, male, C57BL/6) received the drink water with or without citrulline (1 g/kg of body weight) for ~9 weeks. To enhance citrulline supplementation, mice were also orally delivered with a dose of water or water with citrulline (1.5 g/kg of body weight) once a week. Citrulline was purchased from Sigma-Aldrich (C7629). After acclimatization for 1 week, the mice were weighed twice a week and euthanized on day 66. Liver and spleen tissues were weighed. BMDMs were isolated from hind legs. Left brain tissues were harvested for immunohistochemistry, and right brain and liver tissues were used for metabolomics.

LPS challenge experiment

Mice (8 weeks old, female, C57BL/6) were fed with water or water with citrulline (1 g/kg of body weight) for 7 days. To enhance citrulline uptake, these mice were also orally delivered with a dose of water or water with citrulline (1.5 g/kg of body weight) once a day during days 3 to 7. All mice were exposed to LPS challenge on day 7. In the acute liver injury model, mice were treated with LPS (10 μg/kg of body weight) and GalN (500 mg/kg of body weight) through intraperitoneal injection on day 7. In the sepsis model, mice were treated with a lethal dose of LPS (35 mg/kg of body weight) through intraperitoneal injection on day 7. In the third model, mice were treated with a nonlethal dose of LPS (20 mg/kg of body weight) through intraperitoneal injection on day 7. For the survival experiment, mouse survival was observed and recorded every half hour. For low-dose LPS challenge experiment, after 6 hours of LPS treatment, mice were first anesthetized with isoflurane and euthanized. Then, mouse tissues were dissected and immediately frozen using liquid nitrogen.

Immunohistochemistry

Serial brain tissue sections (30 μm) were used for immunohistochemical staining with the following modifications. Briefly, the sections were blocked in tris-buffered saline combined with 1% Triton X-100 and 10% donkey serum for 2 hours. All primary antibodies were used and incubated for 2 days at 4°C. Secondary antibodies were used and incubated for 4 hours at room temperature. Fluorescently stained sections were counterstained with 4′,6-diamidino-2-phenylindole (DAPI; 200 ng/ml; Sigma-Aldrich) for 2 to 5 min and then coverslipped with Gel/Mount (Biomeda).

Cell imaging and qualification

The DNA Damage Assay Kit by γH2AX immunofluorescence (Beyotime Biotechnology, #C2035S) was used to detect the phosphorylation of H2AX following the manufacturer's instructions. Cells were photographed at ×20 magnification using Leica microscope (Germany). Image data qualification of γH2AX was determined by ImageJ for DAPI-labeled nuclei and proteins.

Enzyme-linked immunosorbent assays

Proinflammatory cytokine secretions were quantified using mouse TNFα enzyme-linked immunosorbent assay (ELISA) kit (Proteintech, #EK1222), mouse IL-1β ELISA kit (Proteintech, #EK10002), and mouse IL-6 ELISA kit (Proteintech, #EK10007) according to the manufacturer's instructions.

Induction of senescent immortalized MEFs

We followed the previously reported protocol to prepare senescent immortalized MEFs (iMEFs) (*34*). In detail, iMEFs were subjected to treatment with tBHP at various concentrations for 2 hours, followed by recovery in complete cell culture medium for 3 days. Subsequently, these cells underwent passaging for 4 days to induce cellular senescence.

SA-β-Gal assay

SA-β-Gal activity was measured using SA-β-Gal staining kit (CST, #9860). Briefly, cells were washed with PBS and fixed for 10 min at room temperature in a fixing solution of the SA-β-Gal kit. After washing twice with PBS, cells were incubated in senescence detection solution overnight at 37°C. Subsequently, cells were photographed at ×10 magnification using Olympus CKX53 optical light microscope (Tokyo, Japan). The percentage of SA-β-Gal-positive cells was determined by counting blue-stained cells from three fields of each sample.

Metabolites extraction

For extraction of cellular metabolites, the cell culture medium was quickly removed, and the cells were washed with PBS twice. The cell dishes were placed on dry ice, and the metabolite extraction solution (acetonitrile/methanol/water = 2:2:1, v/v/v; 1 ml) was added to the dishes to quench the metabolism. The extraction solution was precooled at −80°C for 1 hour before the extraction. The plates were then incubated at −80°C for at least 40 min. The cell contents were scraped and transferred to a 1.5-ml Eppendorf tube. The samples were vortexed for 1 min and centrifuged for 10 min at 17,000*g* and 4°C to precipitate the insoluble materials. The supernatant was taken to a new 1.5-ml Eppendorf tube and evaporated to dryness at 4°C using a vacuum concentrator. The dried extracts were kept in −80°C until LC-MS analysis. Before the LC-MS analysis, the dried extracts were reconstituted in 100 μl of acetonitrile/H_2O (1:1, v/v), sonicated for 10 min, and centrifuged for 15 min at 17,000*g* and 4°C to remove insoluble debris. The supernatant was then transferred to high-performance liquid chromatography (HPLC) vials for LC-MS analysis.

For metabolite extraction from tissues, each tissue sample was homogenized by grinding on liquid nitrogen and aliquoted every ~20 mg. Two hundred microliters of water was added into 20 mg of tissue sample for further homogenization. Homogenized tissue solution (200 μl) was extracted using 800 μl of acetonitrile/methanol (1:1, v/v). The samples were vortexed for 30 s and sonicated for 10 min in an ice bath. To precipitate proteins, samples were incubated for 1 hour at −20°C, followed by 15 min of centrifugation at 17,000*g* and 4°C. The dried extracts were kept in −80°C as previously described.

For metabolite extraction from serum, 50 μl of serum sample was extracted using 200 μl acetonitrile/methanol (1:1, v/v). The samples were vortexed for 30 s and sonicated 10 min in an ice bath. To precipitate proteins, the samples were incubated for 1 hour at −20°C, followed by 15 min of centrifugation at 17,500*g* and 4°C. The dried extracts were kept in −80°C as previously described.

For sample normalization, the protein precipitate was reconstituted with 200 μl of lysis buffer [100 mM tris-HCl with 4% (w/v) SDS (pH 7.6)], vortexed for 30 s, and sonicated until the protein solution was generated. Bicinchoninic acid kit was used to determine the protein concentrations in each sample and used as a reference to adjust the volumes of reconstitution buffer for sample reconstitution. Before the LC-MS analysis, the dried extracts were reconstituted with acetonitrile/H_2O (1:1, v/v), sonicated for 10 min, and centrifuged for 15 min at 17,000*g* and 4°C to remove insoluble debris. The supernatant was then transferred to HPLC vials for LC-MS analysis.

Stable-isotope tracing metabolomics

MEF cells or primary BMDM cells were plated in 6-cm dishes at 2,000,000 cells per dish and cultured in arginine-free DMEM containing dialyzed FBS (10%), penicillin/streptomycin (1%), and 400 μM [U-^{13}C]-arginine. For MEFs, cells were first grown to 75 to 80% confluence in the log phase in cell culture plates with normal culture medium. Then, the culture medium was changed to fresh medium with 400 μM [U-^{13}C]-arginine for 24 hours. Fast quench-based extraction of cellular metabolites was performed as previously described. For primary BMDMs, on day 6 of culture, adherent BMDM cells were counted and plated into new wells containing fresh medium with 400 μM [U-^{13}C]-arginine for 24 hours. After that, fast quench-based extraction of cellular metabolites was also performed as previously described.

LC-MS analysis

The untargeted metabolomics analyses of aging mouse brain tissues, liver tissues, and serum followed our previous publication (*75*). Briefly, an ultra-HPLC (UHPLC) system (1290 series, Agilent Technologies, USA) coupled to a quadruple time-of-flight mass spectrometer (TripleTOF 6600, SCIEX, USA) was used for LC-MS analyses. A Waters Ethylene Bridged Hybrid (BEH) amide column was used for LC separation. Mobile phases, linear gradient elution, and electrospray ionization source parameters followed the previous publication (*75*). Other metabolomics analyses followed an updated method in our recent publication (*76*). Briefly, LC-MS analyses were performed using a Vanquish UHPLC coupled to Orbitrap Exploris 480 (Thermo Fisher Scientific, USA). The raw data were acquired using Xcalibur (version 4.4.16.14). A Waters BEH amide column and Phenomenex Kinetex C18 column were used for LC separation for hydrophilic interaction liquid chromatography (HILIC) mode and reversed phase liquid chromatography (RPLC) mode. Mobile phases, linear gradient elution, and electrospray ionization source parameters followed the previous publication (*76*). Metabolomics data analysis and metabolite annotation were performed using MetDNA (http://metdna.zhulab.cn/) (*75*, *77*). Metabolite annotations with confidence level 1 were reported in our study, which were obtained through matching of MS1, retention time (RT), and MS/MS spectra with the experimental metabolite spectral library. Metabolic pathway enrichment analysis was performed via hypergeometric test and visualized in R (v 4.3.0). The pathway database was Kyoto Encyclopedia of Genes and Genomes (www.genome.jp/kegg/). Stable-isotope tracing metabolomics data analysis was performed using MetTracer (*76*).

Measurement of cellular ECAR and OCR

Cellular ECAR and OCR values were measured using the XFe96 Extracellular Flux Analyzer (Agilent Technologies, USA) following the manufacturer's protocols. Briefly, iBMDMs were seeded in XFe96-well microplate with 1.0×10^4 cells per well, pretreated with citrulline (500 μM) for 0.5 hours, and followed by LPS treatment (100 ng/ml) for 4 hours before XF assay. ECAR was measured in XF medium under basal conditions. Glucose (10 mM), oligomycin (5 μM), and 2-deoxyglucose (2-DG; 100 mM; glycolysis inhibitor) were sequentially added to measure glycolysis, glycolysis capacity, and glycolysis reverse, respectively. OCR was measured in XF medium under basal conditions. Oligomycin (1.5 μM), FCCP (carbonyl cyanide *p*-trifluoromethoxyphenylhydrazone; 0.5 μM), and rotenone/antimycin A (0.5 μM) were sequentially added to measure nonmitochondrial oxygen consumption, basal respiration, maximal respiration, proton leak, ATP production, and spare respiratory capacity, respectively.

For normalization of the ECAR and OCR experiments, we counted the cells before seeding to ensure the same cell numbers in each well of a 96-well plate (10,000 iBMDM cells). The reported ECAR values were normalized to the cell numbers. The Seahorse measurements were all performed with the following assay conditions: 3 min of mixing, 3 min of waiting, and 3 min of measurements.

Nonglycolytic acidification, maximum glycolytic capacity, and glycolytic reserve were calculated in the ECAR experiment. Below is the detailed information: nonglycolytic acidification = last rate measurement before glucose injection; maximum glycolytic capacity = (maximum rate measurement before oligomycin injection) − (last rate measurement before glucose injection); glycolytic capacity = (maximum rate measurement after oligomycin injection) − (last rate measurement before glucose injection). Nonmitochondrial oxygen consumption, basal respiration, maximal respiration, proton leak, ATP production, and spare respiratory capacity were calculated in the OCR experiments. Below is the detailed information: nonmitochondrial oxygen consumption = minimum rate measurement after rotenone/antimycin A injection; basal respiration = (last rate measurement before first injection) − (nonmitochondrial respiration rate); maximal respiration = (maximum rate measurement after FCCP injection) − (nonmitochondrial respiration); proton leak = (minimum rate measurement after oligomycin injection) − (nonmitochondrial respiration); ATP production = (last rate measurement before oligomycin injection) − (minimum rate measurement after oligomycin injection); spare respiratory capacity = (maximal respiration) − (basal respiration). The results were analyzed and exported from software Seahorse Wave (version 2.4.0.60).

Real-time polymerase chain reaction
RNA was isolated using TRIzol reagent (Thermo Fisher Scientific, USA) in accordance with manufacturer's instructions. RNA was resuspended in diethyl pyrocarbonate–treated ribonuclease-free water (Thermo Fisher Scientific, USA). Reverse transcription was catalyzed using the SuperScript III First-Strand Synthesis System (Thermo Fisher Scientific, USA). Real-time polymerase chain reaction (PCR) analysis was performed using the QuantStudio 6 Flex real-time PCR system with SYBR Select Master Mix (Thermo Fisher Scientific, USA). We extensively used the $2^{-\Delta\Delta CT}$ method as a relative quantification strategy for quantitative real-time PCR data (*78*). The relative abundance of RNA were calculated based on the $2^{-\Delta\Delta CT}$. $\Delta CT = CT$ (target) − CT (reference, β-actin), $\Delta\Delta CT = CT$ (case) − CT (control), relative abundance of RNA = $2^{-\Delta\Delta CT}$.

PBMC collection
PBMC collection has received ethical approval from the ethical committee of Shanghai Yangpu Hospital, Tongji University School of Medicine with the approval number LL-2022-LW-016. In EDTA-K anticoagulant tubes, 3 ml of whole blood was centrifuged at 4000 rpm for 10 min, yielding the separation of three layers: yellow plasma, white blood cells/platelets, and red blood cells. Plasma was stored at −80°C. Next, 3 ml of PBS was added to the tubes to dilute the blood sample. In a separate tube, 3 ml of Ficoll-Paque reagent (Cytiva, #17544203-1) was equilibrated to room temperature. The diluted blood was carefully layered onto the Ficoll-Paque, avoiding mixing the two solutions, and then centrifuged at 400*g* for 30 min at 25°C, resulting in four layers: diluted plasma, PBMC cell layer, white separating liquid, and red blood cells. The diluted plasma was discarded, and PBMC cell layer was transferred to a new tube. PBMCs were washed twice with 3 ml of PBS. Then, PBMC pellet was washed with 1 ml of PBS, transferred to 2-ml Eppendorf tube, and stored at −80°C.

Statistical analysis
All quantifications of fluorescence images were represented as means ± SEM from three replicates. Quantifications of immunoblots and immunostaining were performed using ImageJ (version 1.8.0). All statistical analyses were performed using GraphPad Prism (v 8.0 and v 9.0), Microsoft Excel 2010, and R (version 3.4.3). All Western blots from cell samples and mouse tissues were repeated at least three times with similar results. Differences were considered to be significant if $P < 0.05$.

Supplementary Materials
The PDF file includes:
Figs. S1 to S6
Tables S1 and S2
Legends for data S1 to S3

Other Supplementary Material for this manuscript includes the following:
Data S1 to S3

REFERENCES AND NOTES

1. B. K. Kennedy, S. L. Berger, A. Brunet, J. Campisi, A. M. Cuervo, E. S. Epel, C. Franceschi, G. J. Lithgow, R. I. Morimoto, J. E. Pessin, T. A. Rando, A. Richardson, E. E. Schadt, T. Wyss-Coray, F. Sierra, Geroscience: Linking aging to chronic disease. *Cell* **159**, 709–713 (2014).
2. C. Lopez-Otin, L. Galluzzi, J. M. P. Freije, F. Madeo, G. Kroemer, Metabolic control of longevity. *Cell* **166**, 802–821 (2016).
3. C. Lopez-Otin, M. A. Blasco, L. Partridge, M. Serrano, G. Kroemer, Hallmarks of aging: An expanding universe. *Cell* **186**, 243–278 (2023).
4. J. Ding, J. Ji, Z. Rabow, T. Shen, J. Folz, C. R. Brydges, S. Fan, X. Lu, S. Mehta, M. R. Showalter, Y. Zhang, R. Araiza, L. R. Bower, K. C. K. Lloyd, O. Fiehn, A metabolome atlas of the aging mouse brain. *Nat. Commun.* **12**, 6021 (2021).
5. M. Savini, A. Folick, Y. T. Lee, F. Jin, A. Cuevas, M. C. Tillman, J. D. Duffy, Q. Zhao, I. A. Neve, P. W. Hu, Y. Yu, Q. Zhang, Y. Ye, W. B. Mair, J. Wang, L. Han, E. A. Ortlund, M. C. Wang, Lysosome lipid signalling from the periphery to neurons regulates longevity. *Nat. Cell Biol.* **24**, 906–916 (2022).
6. D. Li, Y. Ke, R. Zhan, C. Liu, M. Zhao, A. Zeng, X. Shi, L. Ji, S. Cheng, B. Pan, L. Zheng, H. Hong, Trimethylamine-N-oxide promotes brain aging and cognitive impairment in mice. *Aging Cell* **17**, e12768 (2018).
7. Z. Wang, E. Klipfell, B. J. Bennett, R. Koeth, B. S. Levison, B. DuGar, A. E. Feldstein, E. B. Britt, X. Fu, Y. M. Chung, Y. Wu, P. Schauer, J. D. Smith, H. Allayee, W. H. W. Tang, J. A. DiDonato, A. J. Lusis, S. L. Hazen, Gut flora metabolism of phosphatidylcholine promotes cardiovascular disease. *Nature* **472**, 57–63 (2011).
8. A. M. Fretts, S. L. Hazen, P. Jensen, M. Budoff, C. M. Sitlani, M. Wang, M. C. de Oliveira Otto, J. A. DiDonato, Y. Lee, B. M. Psaty, D. S. Siscovick, N. Sotoodehnia, W. H. W. Tang, H. Lai, R. N. Lemaitre, D. Mozaffarian, Association of trimethylamine N-oxide and metabolites with mortality in older adults. *JAMA Netw. Open* **5**, e2213242 (2022).
9. E. F. Fang, S. Lautrup, Y. Hou, T. G. Demarest, D. L. Croteau, M. P. Mattson, V. A. Bohr, NAD+ in aging: Molecular mechanisms and translational implications. *Trends Mol. Med.* **23**, 899–916 (2017).
10. K. Yaku, K. Okabe, T. Nakagawa, NAD metabolism: Implications in aging and longevity. *Ageing Res. Rev.* **47**, 1–17 (2018).
11. S. Lautrup, D. A. Sinclair, M. P. Mattson, E. F. Fang, NAD^+ in brain aging and neurodegenerative disorders. *Cell Metab.* **30**, 630–655 (2019).
12. H. Nadeeshani, J. Li, T. Ying, B. Zhang, J. Lu, Nicotinamide mononucleotide (NMN) as an anti-aging health product–promises and safety concerns. *J. Adv. Res.* **37**, 267–278 (2022).
13. L. Yi, A. B. Maier, R. Tao, Z. Lin, A. Vaidya, S. Pendse, S. Thasma, N. Andhalkar, G. Avhad, V. Kumbhar, The efficacy and safety of β-nicotinamide mononucleotide (NMN) supplementation in healthy middle-aged adults: A randomized, multicenter, double-blind, placebo-controlled, parallel-group, dose-dependent clinical trial. *Geroscience* **45**, 29–43 (2023).
14. P. Singh, K. Gollapalli, S. Mangiola, D. Schranner, M. A. Yusuf, M. Chamoli, S. L. Shi, B. Lopes Bastos, T. Nair, A. Riermeier, E. M. Vayndorf, J. Z. Wu, A. Nilakhe, C. Q. Nguyen, M. Muir, M. G. Kiflezghi, A. Foulger, A. Junker, J. Devine, K. Sharan, S. J. Chinta, S. Rajput, A. Rane, P. Baumert, M. Schönfelder, F. Iavarone, G. di Lorenzo, S. Kumari, A. Gupta, R. Sarkar, C. Khyriem, A. S. Chawla, A. Sharma, N. Sarper, N. Chattopadhyay, B. K. Biswal, C. Settembre, P. Nagarajan, K. L. Targoff, M. Picard, S. Gupta, V. Velagapudi, A. T. Papenfuss, A. Kaya, M. G. Ferreira, B. K. Kennedy, J. K. Andersen, G. J. Lithgow, A. M. Ali, A. Mukhopadhyay, A. Palotie, G. Kastenmüller, M. Kaeberlein, H. Wackerhage, B. Pal, V. K. Yadav, Taurine deficiency as a driver of aging. *Science* **380**, eabn9257 (2023).
15. F. Madeo, T. Eisenberg, F. Pietrocola, G. Kroemer, Spermidine in health and disease. *Science* **359**, eaan2788 (2018).
16. S. Kiechl, R. Pechlaner, P. Willeit, M. Notdurfter, B. Paulweber, K. Willeit, P. Werner, C. Ruckenstuhl, B. Iglseder, S. Weger, B. Mairhofer, M. Gartner, L. Kedenko, M. Chmelikova, S. Stekovic, H. Stuppner, F. Oberhollenzer, G. Kroemer, M. Mayr, T. Eisenberg, H. Tilg, F. Madeo, J. Willeit, Higher spermidine intake is linked to lower mortality: A prospective population-based study. *Am. J. Clin. Nutr.* **108**, 371–380 (2018).
17. D. S. Wishart, Metabolomics for investigating physiological and pathophysiological processes. *Physiol. Rev.* **99**, 1819–1875 (2019).
18. C. Franceschi, P. Garagnani, P. Parini, C. Giuliani, A. Santoro, Inflammaging: A new immune–metabolic viewpoint for age-related diseases. *Nat. Rev. Endocrinol.* **14**, 576–590 (2018).
19. L. Ferrucci, E. Fabbri, Inflammageing: Chronic inflammation in ageing, cardiovascular disease, and frailty. *Nat. Rev. Cardiol.* **15**, 505–522 (2018).
20. F. Pietrocola, J. Pol, E. Vacchelli, S. Rao, D. P. Enot, E. E. Baracco, S. Levesque, F. Castoldi, N. Jacquelot, T. Yamazaki, L. Senovilla, G. Marino, F. Aranda, S. Durand, V. Sica, A. Chery, S. Lachkar, V. Sigl, N. Bloy, A. Buque, S. Falzoni, B. Ryffel, L. Apetoh, F. di Virgilio, F. Madeo, M. C. Maiuri, L. Zitvogel, B. Levine, J. M. Penninger, G. Kroemer, Caloric restriction mimetics enhance anticancer immunosurveillance. *Cancer Cell* **30**, 147–160 (2016).
21. A. Asadi Shahmirzadi, D. Edgar, C. Y. Liao, Y. M. Hsu, M. Lucanic, A. Asadi Shahmirzadi, C. D. Wiley, G. Gan, D. E. Kim, H. G. Kasler, C. Kuehnemann, B. Kaplowitz, D. Bhaumik, R. R. Riley, B. K. Kennedy, G. J. Lithgow, Alpha-ketoglutarate, an endogenous metabolite, extends lifespan and compresses morbidity in aging mice. *Cell Metab.* **32**, 447–456.e6 (2020).
22. E. Montecino-Rodriguez, B. Berent-Maoz, K. Dorshkind, Causes, consequences, and reversal of immune system aging. *J. Clin. Invest.* **123**, 958–965 (2013).
23. A. A. van Beek, J. van den Bossche, P. G. Mastroberardino, M. P. J. de Winther, P. J. M. Leenen, Metabolic alterations in aging macrophages: Ingredients for inflammaging? *Trends Immunol.* **40**, 113–127 (2019).

24. T. A. Wynn, A. Chawla, J. W. Pollard, Macrophage biology in development, homeostasis and disease. *Nature* **496**, 445–455 (2013).
25. J. V. Price, R. E. Vance, The macrophage paradox. *Immunity* **41**, 685–693 (2014).
26. J. Plowden, M. Renshaw-Hoelscher, C. Engleman, J. Katz, S. Sambhara, Innate immunity in aging: Impact on macrophage function. *Aging Cell* **3**, 161–167 (2004).
27. S. Mahbub, C. R. Deburghgraeve, E. J. Kovacs, Advanced age impairs macrophage polarization. *J. Interferon Cytokine Res.* **32**, 18–26 (2012).
28. J.-M. Cavaillon, M. Adib-Conquy, Bench-to-bedside review: Endotoxin tolerance as a model of leukocyte reprogramming in sepsis. *Crit. Care* **10**, 233 (2006).
29. P. H. Li, R. Zhang, L. Q. Cheng, J. J. Liu, H. Z. Chen, Metabolic regulation of immune cells in proinflammatory microenvironments and diseases during ageing. *Ageing Res. Rev.* **64**, 101165 (2020).
30. L. Ginaldi, M. F. Loreto, M. P. Corsi, M. Modesti, M. de Martinis, Immunosenescence and infectious diseases. *Microbes Infect.* **3**, 851–857 (2001).
31. M. Funasako, M. Taniji, K. Fujimoto, M. Ohata, Y. Higashimoto, K. Uetani, T. Suruda, S. Nakai, H. Fujimoto, Y. Sakagami, Effect of aging on plasma 1,5-anhydroglucitol levels in humans and rats. *Diabetes Res. Clin. Pract.* **25**, 35–41 (1994).
32. I. K. Cheah, L. Feng, R. M. Y. Tang, K. H. C. Lim, B. Halliwell, Ergothioneine levels in an elderly population decrease with age and incidence of cognitive decline; a risk factor for neurodegeneration? *Biochem. Biophys. Res. Commun.* **478**, 162–167 (2016).
33. L. Verbruggen, G. Ates, O. Lara, J. de Munck, A. Villers, L. de Pauw, S. Ottestad-Hansen, S. Kobayashi, P. Beckers, P. Janssen, H. Sato, Y. Zhou, E. Hermans, R. Njemini, L. Arckens, N. C. Danbolt, D. de Bundel, J. L. Aerts, K. Barbé, B. Guillaume, L. Ris, E. Bentea, A. Massie, Lifespan extension with preservation of hippocampal function in aged system x_c^--deficient male mice. *Mol. Psychiatry* **27**, 2355–2368 (2022).
34. D. Volonte, H. Zou, J. N. Bartholomew, Z. Liu, P. A. Morel, F. Galbiati, Oxidative stress-induced inhibition of Sirt1 by caveolin-1 promotes p53-dependent premature senescence and stimulates the secretion of interleukin 6 (IL-6). *J. Biol. Chem.* **290**, 4202–4214 (2015).
35. M. Ogrodnik, S. Miwa, T. Tchkonia, D. Tiniakos, C. L. Wilson, A. Lahat, C. P. Day, A. Burt, A. Palmer, Q. M. Anstee, S. N. Grellscheid, J. H. J. Hoeijmakers, S. Barnhoorn, D. A. Mann, T. G. Bird, W. P. Vermeij, J. L. Kirkland, J. F. Passos, T. von Zglinicki, D. Jurk, Cellular senescence drives age-dependent hepatic steatosis. *Nat. Commun.* **8**, 15691 (2017).
36. M. Y. Ou, H. Zhang, P. C. Tan, S. B. Zhou, Q. F. Li, Adipose tissue aging: Mechanisms and therapeutic implications. *Cell Death Dis.* **13**, 300 (2022).
37. Y. Ovadya, T. Landsberger, H. Leins, E. Vadai, H. Gal, A. Biran, R. Yosef, A. Sagiv, A. Agrawal, A. Shapira, J. Windheim, M. Tsoory, R. Schirmbeck, I. Amit, H. Geiger, V. Krizhanovsky, Impaired immune surveillance accelerates accumulation of senescent cells and aging. *Nat. Commun.* **9**, 5435 (2018).
38. D. Frasca, B. B. Blomberg, R. Paganelli, Aging, obesity, and inflammatory age-related diseases. *Front. Immunol.* **8**, 324042 (2017).
39. M. F. Gregor, G. S. Hotamisligil, Inflammatory mechanisms in obesity. *Annu. Rev. Immunol.* **29**, 415–445 (2011).
40. S. Pfeiffer, E. Leopold, K. Schmidt, F. Brunner, B. Mayer, Inhibition of nitric oxide synthesis by NG-nitro-L-arginine methyl ester (L-NAME): Requirement for bioactivation to the free acid, NG-nitro-L-arginine. *Br. J. Pharmacol.* **118**, 1433–1440 (1996).
41. A. Mori, M. Morita, K. Morishita, K. Sakamoto, T. Nakahara, K. Ishii, L-Citrulline dilates rat retinal arterioles via nitric oxide-and prostaglandin-dependent pathways in vivo. *J. Pharmacol. Sci.* **127**, 419–423 (2015).
42. Y. Hu, Y. Xu, L. Mao, W. Lei, J. Xiang, L. Gao, J. Jiang, L. A. Huang, O. J. Luo, J. Duan, G. Chen, Gene expression analysis reveals age and ethnicity signatures between young and old adults in human PBMC. *Front. Aging* **2**, 797040 (2022).
43. E. Curis, I. Nicolis, C. Moinard, S. Osowska, N. Zerrouk, S. Bénazeth, L. Cynober, Almost all about citrulline in mammals. *Amino Acids* **29**, 177–205 (2005).
44. I. Ceballos, P. Chauveau, V. Guerin, J. Bardet, P. Parvy, P. Kamoun, P. Jungers, Early alterations of plasma free amino acids in chronic renal failure. *Clin. Chim. Acta* **188**, 101–108 (1990).
45. P. S. Minhas, A. Latif-Hernandez, M. R. McReynolds, A. S. Durairaj, Q. Wang, A. Rubin, A. U. Joshi, J. Q. He, E. Gauba, L. Liu, C. Wang, M. Linde, Y. Sugiura, P. K. Moon, R. Majeti, M. Suematsu, D. Mochly-Rosen, I. L. Weissman, F. M. Longo, J. D. Rabinowitz, K. I. Andreasson, Restoring metabolism of myeloid cells reverses cognitive decline in ageing. *Nature* **590**, 122–128 (2021).
46. Z. Liu, W. Li, L. Geng, L. Sun, Q. Wang, Y. Yu, P. Yan, C. Liang, J. Ren, M. Song, Q. Zhao, J. Lei, Y. Cai, J. Li, K. Yan, Z. Wu, Q. Chu, J. Li, S. Wang, C. Li, J. D. J. Han, R. Hernandez-Benitez, N. Shyh-Chang, J. C. I. Belmonte, W. Zhang, J. Qu, G. H. Liu, Cross-species metabolomic analysis identifies uridine as a potent regeneration promoting factor. *Cell Discov.* **8**, 6 (2022).
47. R. A. Saxton, D. M. Sabatini, mTOR Signaling in growth, metabolism, and disease. *Cell* **168**, 960–976 (2017).
48. D. Papadopoli, K. Boulay, L. Kazak, M. Pollak, F. Mallette, I. Topisirovic, L. Hulea, mTOR as a central regulator of lifespan and aging. *F1000Res* **8**, F1000 Faculty Rev-998 (2019).
49. J. J. Wu, J. Liu, E. B. Chen, J. J. Wang, L. Cao, N. Narayan, M. M. Fergusson, I. I. Rovira, M. Allen, D. A. Springer, C. U. Lago, S. Zhang, W. DuBois, T. Ward, R. deCabo, O. Gavrilova, B. Mock, T. Finkel, Increased mammalian lifespan and a segmental and tissue-specific slowing of aging after genetic reduction of mTOR expression. *Cell Rep.* **4**, 913–920 (2013).
50. S. C. Johnson, P. S. Rabinovitch, M. Kaeberlein, mTOR is a key modulator of ageing and age-related disease. *Nature* **493**, 338–345 (2013).
51. S. Robida-Stubbs, K. Glover-Cutter, D. W. Lamming, M. Mizunuma, S. D. Narasimhan, E. Neumann-Haefelin, D. M. Sabatini, T. K. Blackwell, TOR signaling and rapamycin influence longevity by regulating SKN-1/Nrf and DAF-16/FoxO. *Cell Metab.* **15**, 713–724 (2012).
52. I. Bjedov, J. M. Toivonen, F. Kerr, C. Slack, J. Jacobson, A. Foley, L. Partridge, Mechanisms of life span extension by rapamycin in the fruit fly *Drosophila melanogaster*. *Cell Metab.* **11**, 35–46 (2010).
53. D. E. Harrison, R. Strong, Z. D. Sharp, J. F. Nelson, C. M. Astle, K. Flurkey, N. L. Nadon, J. E. Wilkinson, K. Frenkel, C. S. Carter, M. Pahor, M. A. Javors, E. Fernandez, R. A. Miller, Rapamycin fed late in life extends lifespan in genetically heterogeneous mice. *Nature* **460**, 392–395 (2009).
54. A. Bitto, T. K. Ito, V. V. Pineda, N. J. LeTexier, H. Z. Huang, E. Sutlief, H. Tung, N. Vizzini, B. Chen, K. Smith, D. Meza, M. Yajima, R. P. Beyer, K. F. Kerr, D. J. Davis, C. H. Gillespie, J. M. Snyder, P. M. Treuting, M. Kaeberlein, Transient rapamycin treatment can increase lifespan and healthspan in middle-aged mice. *eLife* **5**, e16351 (2016).
55. R. A. Saxton, L. Chantranupong, K. E. Knockenhauer, T. U. Schwartz, D. M. Sabatini, Mechanism of arginine sensing by CASTOR1 upstream of mTORC1. *Nature* **536**, 229–233 (2016).
56. L. Chantranupong, S. M. Scaria, R. A. Saxton, M. P. Gygi, K. Shen, G. A. Wyant, T. Wang, J. W. Harper, S. P. Gygi, D. M. Sabatini, The CASTOR proteins are arginine sensors for the mTORC1 pathway. *Cell* **165**, 153–164 (2016).
57. R. A. Saxton, K. E. Knockenhauer, R. L. Wolfson, L. Chantranupong, M. E. Pacold, T. Wang, T. U. Schwartz, D. M. Sabatini, Structural basis for leucine sensing by the Sestrin2-mTORC1 pathway. *Science* **351**, 53–58 (2016).
58. R. L. Wolfson, L. Chantranupong, R. A. Saxton, K. Shen, S. M. Scaria, J. R. Cantor, D. M. Sabatini, Sestrin2 is a leucine sensor for the mTORC1 pathway. *Science* **351**, 43–48 (2016).
59. X. Gu, J. M. Orozco, R. A. Saxton, K. J. Condon, G. Y. Liu, P. A. Krawczyk, S. M. Scaria, J. W. Harper, S. P. Gygi, D. M. Sabatini, SAMTOR is an S-adenosylmethionine sensor for the mTORC1 pathway. *Science* **358**, 813–818 (2017).
60. R. A. Miller, G. Buehner, Y. Chang, J. M. Harper, R. Sigler, M. Smith-Wheelock, Methionine-deficient diet extends mouse lifespan, slows immune and lens aging, alters glucose, T4, IGF-I and insulin levels, and increases hepatocyte MIF levels and stress resistance. *Aging Cell* **4**, 119–125 (2005).
61. N. E. Richardson, E. N. Konon, H. S. Schuster, A. T. Mitchell, C. Boyle, A. C. Rodgers, M. Finke, L. R. Haider, D. Yu, V. Flores, H. H. Pak, S. Ahmad, S. Ahmed, A. Radcliff, J. Wu, E. M. Williams, L. Abdi, D. S. Sherman, T. A. Hacker, D. W. Lamming, Lifelong restriction of dietary branched-chain amino acids has sex-specific benefits for frailty and life span in mice. *Nat. Aging* **1**, 73–86 (2021).
62. S. Le Plénier, A. Goron, A. Sotiropoulos, E. Archambault, C. Guihenneuc, S. Walrand, J. Salles, M. Jourdan, N. Neveux, L. Cynober, C. Moinard, Citrulline directly modulates muscle protein synthesis via the PI3K/MAPK/4E-BP1 pathway in a malnourished state: Evidence from in vivo, ex vivo, and in vitro studies. *J. Physiol. Endocrinol. Metab.* **312**, E27–E36 (2017).
63. S. M. Morris Jr., Regulation of enzymes of the urea cycle and arginine metabolism. *Annu. Rev. Nutr.* **22**, 87–105 (2002).
64. S. N. Kaore, H. S. Amane, N. M. Kaore, Citrulline: Pharmacological perspectives and its role as an emerging biomarker in future. *Fundam. Clin. Pharmacol.* **27**, 35–50 (2013).
65. F. Holguin, H. Grasemann, S. Sharma, D. Winnica, K. Wasil, V. Smith, M. H. Cruse, N. Perez, E. Coleman, T. J. Scialla, L. G. Que, L-Citrulline increases nitric oxide and improves control in obese asthmatics. *JCI Insight* **4**, e131733 (2019).
66. J. Perez-Guisado, P. M. Jakeman, Citrulline malate enhances athletic anaerobic performance and relieves muscle soreness. *J. Strength Cond. Res.* **24**, 1215–1222 (2010).
67. A. Figueroa, A. Wong, S. J. Jaime, J. U. Gonzales, Influence of L-citrulline and watermelon supplementation on vascular function and exercise performance. *Curr. Opin. Clin. Nutr. Metab. Care* **20**, 92–98 (2017).
68. L. Cormio, M. de Siati, F. Lorusso, O. Selvaggio, L. Mirabella, F. Sanguedolce, G. Carrieri, Oral L-citrulline supplementation improves erection hardness in men with mild erectile dysfunction. *Urology* **77**, 119–122 (2011).
69. B. Barkhidarian, S. Seyedhamzeh, S. I. Hashemi, M. Nematy, A. Rahbar, R. Ranjbar, M. Safarian, Effects of arginine and citrulline supplementation on inflammatorymarkers in critically ill patients. *J. Nutr. Sci. & Diet.* **2**, 34–39 (2016).
70. S. Azizi, R. Mahdavi, M. Mobasseri, S. Aliasgharzadeh, F. Abbaszadeh, M. Ebrahimi-Mameghani, The impact of L-citrulline supplementation on glucose homeostasis, lipid profile, and some inflammatory factors in overweight and obese

patients with type 2 diabetes: A double-blind randomized placebo-controlled trial. *Phytother. Res.* **35**, 3157–3166 (2021).
71. Y. Mao, D. Shi, G. Li, P. Jiang, Citrulline depletion by ASS1 is required for proinflammatory macrophage activation and immune responses. *Mol. Cell* **82**, 527–541.e7 (2022).
72. J. E. Qualls, C. Subramanian, W. Rafi, A. M. Smith, L. Balouzian, A. A. DeFreitas, K. A. Shirey, B. Reutterer, E. Kernbauer, S. Stockinger, T. Decker, I. Miyairi, S. N. Vogel, P. Salgame, C. O. Rock, P. J. Murray, Sustained generation of nitric oxide and control of mycobacterial infection requires argininosuccinate synthase 1. *Cell Host Microbe* **12**, 313–323 (2012).
73. A. Hooftman, C. G. Peace, D. G. Ryan, E. A. Day, M. Yang, A. F. McGettrick, M. Yin, E. N. Montano, L. Huo, J. E. Toller-Kawahisa, V. Zecchini, T. A. J. Ryan, A. Bolado-Carrancio, A. M. Casey, H. A. Prag, A. S. H. Costa, G. de Los Santos, M. Ishimori, D. J. Wallace, S. Venuturupalli, E. Nikitopoulou, N. Frizzell, C. Johansson, A. von Kriegsheim, M. P. Murphy, C. Jefferies, C. Frezza, L. A. J. O'Neill, Macrophage fumarate hydratase restrains mtRNA-mediated interferon production. *Nature* **615**, 490–498 (2023).
74. G. L. Seim, E. C. Britt, S. V. John, F. J. Yeo, A. R. Johnson, R. S. Eisenstein, D. J. Pagliarini, J. Fan, Two-stage metabolic remodelling in macrophages in response to lipopolysaccharide and interferon-γ stimulation. *Nat. Metab.* **1**, 731–742 (2019).
75. X. Shen, R. Wang, X. Xiong, Y. Yin, Y. Cai, Z. Ma, N. Liu, Z. J. Zhu, Metabolic reaction network-based recursive metabolite annotation for untargeted metabolomics. *Nat. Commun.* **10**, 1516 (2019).
76. R. Wang, Y. Yin, J. Li, H. Wang, W. Lv, Y. Gao, T. Wang, Y. Zhong, Z. Zhou, Y. Cai, X. Su, N. Liu, Z. J. Zhu, Global stable-isotope tracing metabolomics reveals system-wide metabolic alternations in aging *Drosophila*. *Nat. Commun.* **13**, 3518 (2022).
77. Z. Zhou, M. Luo, H. Zhang, Y. Yin, Y. Cai, Z. J. Zhu, Metabolite annotation from knowns to unknowns through knowledge-guided multi-layer metabolic networking. *Nat. Commun.* **13**, 6656 (2022).
78. K. J. Livak, T. D. Schmittgen, Analysis of relative gene expression data using real-time quantitative PCR and the $2^{-\Delta\Delta CT}$ method. *Methods* **25**, 402–408 (2001).

Acknowledgments
Funding: The work was supported by Strategic Priority Research Program of the Chinese Academy of Sciences (XDB39050700 to Z.-J.Z.), National Natural Science Foundation of China (22425404 and 92357308 to Z.-J.Z.), National Key R&D Program of China (2022YFC3400702 to Z.-J.Z.), Shanghai Key Laboratory of Aging Studies (19DZ2260400 to Z.-J.Z.), Shanghai Municipal Science and Technology Major Project (to Z.-J.Z.), Shanghai Basic Research Pioneer Project (to Z.-J.Z.), National Natural Science Foundation of China (82171288 to X.M.), Shanghai Municipal Natural Science Foundation General Project (22ZR1458100 to X.M.), and Shanghai Municipal Health Commission Health Industry Clinical Research Special Project (20214Y0238 to X.M.). **Author contributions:** Conceptualization: Z.-J.Z., Z.X., and X.M. Methodology: Z.-J.Z., X.M., H.Z., and H.W. Investigation: Z.-J.Z., Z.X., M.L., X.M., H.Z., and H.W. Data curation: Z.-J.Z., H.Z., and H.W. Validation: Z.X., M.L., X.M., H.Z., H.W., Z.C., and B.X. Formal analysis: Z.X., M.L., H.Z., and H.W. Software: X.M., H.Z., and H.W. Resources: Z.-J.Z., Z.X., M.L. H.Z., H.W., and X.M. Visualization: Z.-J.Z., Z.X., M.L. H.Z., H.W., and X.M. Supervision: Z.-J.Z., X.M., and M.L. Project administration: Z.-J.Z. and X.M. Writing—original draft: Z.-J.Z., Z.X., M.L., and X.M. Writing—review and editing: Z.-J.Z., Z.X., M.L., and X.M. Funding acquisition: Z.-J.Z. and X.M. **Competing interests:** The authors declare that they have no competing interests. **Data and materials availability:** All data needed to evaluate the conclusions in the paper are present in the paper and/or the Supplementary Materials. The raw data files of metabolomics data generated in this study have been deposited and are available in the National Omics Data Encyclopedia under accession code OEP004217 (www.biosino.org/node/project/detail/OEP004217). The metabolite identification and quantification results generated in this study are provided in data S1 to S3.

Submitted 18 August 2024
Accepted 31 January 2025
Published 7 March 2025
10.1126/sciadv.ads4957